Utrecht University

The Pliocene-Pleistocene transition in the Kura Basin: Environmental and climate reconstruction of basin margin sediments

Max Bouwmeester - Paleomagnetic Laboratory Fort Hoofddijk, Utrecht University

Advisors: *Liesbeth Jorissen* *(Utrecht University)*
Dr. João Alexandre-Trabucho *(Utrecht University)*
Prof. dr. Wout Krijgsman *(Utrecht University)*

MSc. Thesis - Utrecht University
October 2020

Abstract

During the Neogene, the Caspian Sea experienced major fluctuations in lake-level as a result of climate change and (dis)connections with adjacent basins. A five-fold increase in Caspian Sea surface area is reported to have occurred during the Akchagylian flooding (Plio-Pleistocene). This largest and last flooding is increasingly better understood through research in the Paleo-Kura Basin, a former embayment of the Caspian Sea. These studies focused on the distal and interior parts of the Kura Basin however, leaving the exact expression and timing of the Akchagylian flooding at the basin margin unresolved. This study aims to determine the expression of this flooding and drivers of environmental change in the westernmost extent of the Kura Basin across the Plio-Pleistocene transition. Environmental reconstructions using facies analysis and grainsize distribution limit the maximum westward extent of the Caspian Sea to the location of the studied sections. The muddy, vegetated, and protected coast remained at a relatively constant location by balanced (sub)basin subsidence and sediment supply. An exploratory climate reconstruction using clay mineralogic proxy's for humidity and temperature allows for the identification of three regional to global cooling-warming cycles that might correspond to obliquity-scale orbital forcing. Warm and humid periods increased the deposition of coarser sand-rich sediments, while cold and arid phases are dominated by the deposition of fine-grained mudstones. Tectonic activity of the Kura fold-thrust belt seems to become increasingly more important in controlling sedimentation from the start of the Pleistocene Insights from this study on basin margin sedimentology and clay mineralogy contribute to a better understanding of environmental change in semi-enclosed basins during climate variability, by providing a detailed reconstruction of the largest flooding in the history of the largest 'lake' in the world.

1. Introduction

The Pontocaspian region in the Pliocene-Pleistocene documented a complex history of (dis)connection events between the Caspian Sea, the Black Sea and the open ocean. Major fluctuations in lake-level occurred in these (semi-) isolated basins, greatly impacting their paleo-environmental evolution (Popov et al. 2006; Krijgsman et al. 2019). Mostly isolated from the Black Sea and other Paratethyan basins since the latest Miocene (Reynolds et al. 1998; Gillet et al., 2007; Krijgsman et al. 2010; Munteanu et al. 2012), the Caspian Sea recorded several major lake-level fluctuations throughout the Pliocene-Pleistocene. These are largely documented in the 20-25 km of sediments accumulated in the South Caspian Basin depression (Guliyev et al. 1991; Inan et al. 1997) and along onshore outcrops around the Kura Basin, its former western extension (Lazarev et al. 2019; Jorissen et al. 2019; van Baak et al. 2013; Forte et al. 2015) (Fig. 1a). The Pliocene-Pleistocene Akchagylian regional stage documented a major flooding event with the deposition of offshore mudstones enriched in marine and brackish water fauna. During this flooding, the Caspian Sea surface area is believed to have increased five-fold compared to the preceding Productive Series regional stage lowstand. This major transgression is thought to be driven by an oceanic arctic connection subsequent to the intensification of glaciations in the Northern Hemisphere (Naidina & Richards 2018; van Baak et al. 2019).

Presently, the Caspian Sea is experiencing fluctuations in lake-level that occur a factor two faster than global ocean change (Leroy et al. 2018; Arpe et al. 2000; Kroonenberg et al. 2007; Molavi-Arabshahi et al. 2016), in responsible for the recent biodiversity crisis in the Pontocaspian region (Van de Velde et al. 2019). Understanding the past response of basin margins to such changes is crucial for identifying present challenges in the region, then and now occurring during a time known for rapid climate change (Lisiecki and Raymo 2007; Sosdian and Rosenthal 2009; Haughton, Jenkins and Ephraums 1990). Where human activity nowadays has severe effects on the Caspian Sea region (Nouri, Karbasi and Mirkia 2009; Yanina, Svitoch and Wesselingh 2010), the changes during the Pliocene-Pleistocene transition likely had major effects on the first homonids that migrated out of Africa (Gabunia et al. 2000; Vekua et al. 2002). In fact, the Kvabebi locality in this research is one of the famous homonid excavation sites in Georgia (Agusti et al. 2009). Understanding environmental conditions during this time of migration may provide valuable insight in this important chapter in homonid -and thus human- evolution.

The extent of lake-level fluctuations and their impacts along the paleocoastline of the Caspian Basin are still not fully resolved due to few well-exposed and continuous sedimentary successions covering the Plio-Pleistocene. This research aims therefore to characterise the Pliocene-Pleistocene environmental changes along the Kura Basin margins, based on two continuous and well-exposed onshore sections in its westernmost extent. To determine the extent of the Caspian Sea ingression into the Kura Basin, an environmental reconstruction is presented using sedimentary facies characterisation and association, combined with grainsize analyses to identify depositional environments. Paleoclimatic conditions are reconstructed using clay mineralogy to investigate temperature and humidity effects on environmental

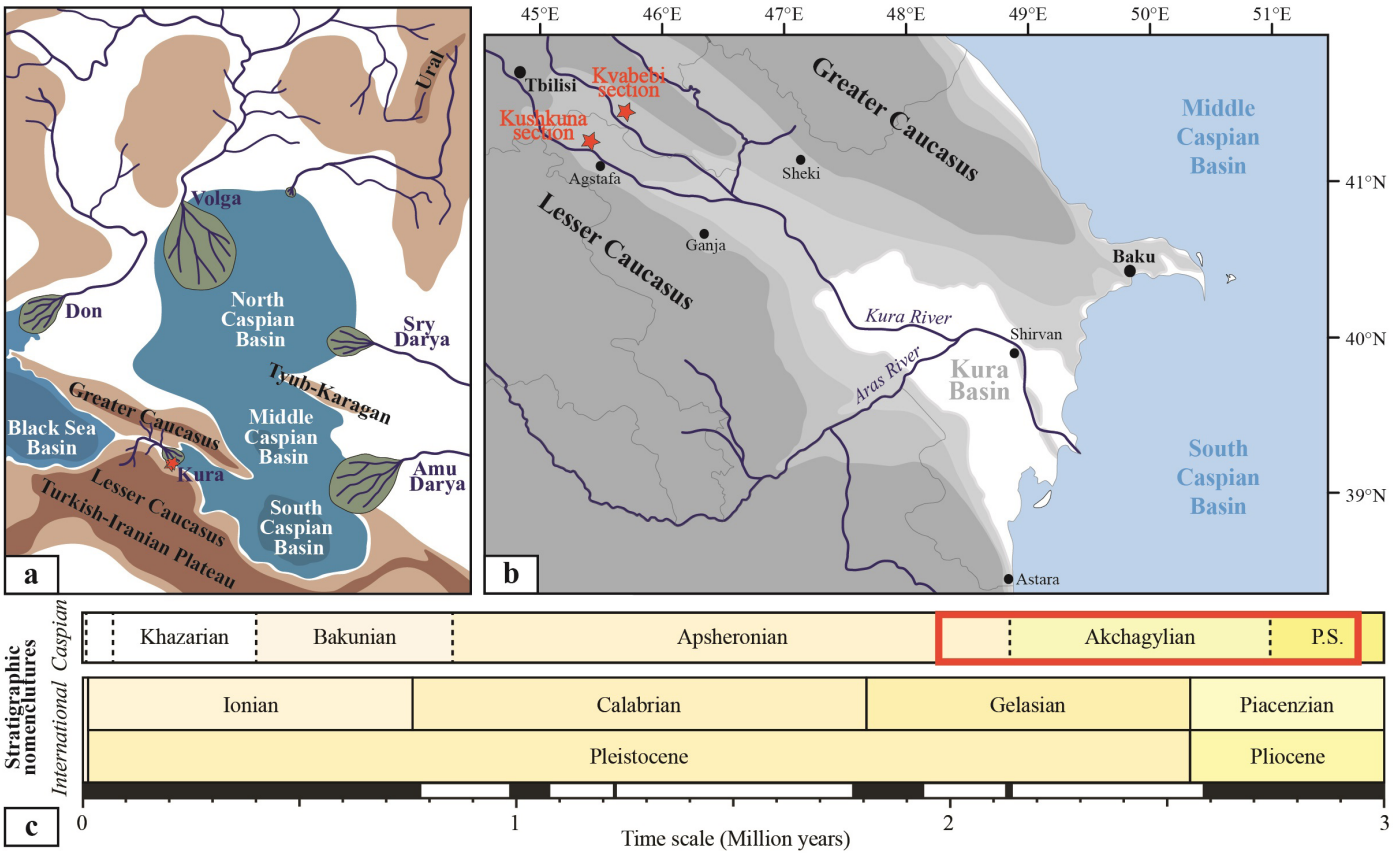

Figure 1: a) Paleoenvironmental map of the Caspian Sea basins and associated sediment supply systems during the Plio-Pleistocene (modified after Jorissen et al., forthcoming). **b)** Geographical map of the Kura Basin, western embayment of the South Caspian Basin, with contemporary rivers and coastline. Localizations of the the Kvabebi (Georgia) and Kushuna (Azerbaijan) sections indicated by red stars. **c)** Stratigraphic chart of the Pontocaspian regional stages correlated to the international nomenclature (modified after Krijgsman et al. 2019).

changes, giving further information on weathering patterns and characteristics of the provenance area. This study explores the use of clay mineralogy in continental settings, whereas the technique was previously mainly applied to marine settings.

This research shows that the Caspian Sea transgression barely reached the location of the studied sections. The paleo-coastline remained at or close to the location of the sections during this episode of the Akchagylian highstand phase, suggesting that sediment supply was balanced with subsidence of the basin margin. The climate signal in sediments near this muddy, protected and vegetated coast suggests that climatic conditions prevailed on a scale outstretching the Caucasus region, and controlled sediment supply patterns in the Kura Basin margin. The use of continental clay mineralogy for climate reconstruction seems successfully executed and the results are promising for future research.

2. Regional setting

The Kura Basin is a former sub-basin of the southwest Caspian Sea Basin (Fig. 1a). This embayment has a north-west to south-east orientation and corresponds to the foreland basin of both the Greater Caucasus in the north and the Lesser Caucasus in the south. These mountain ranges formed during an orogenic episode following the continent-continent collision of Africa-Arabia and Eurasia initiated during the Oligocene (Vincent et al. 2007). This resulted during the Mesozoic-Early Cenozoic in an inversion of the back-arc basin that preceded the Greater Caucasus (Saintot et al. 2006), the active margin basin preceding the Lesser Caucasus (Sosson et al. 2010) and numerous island-arc and rift basins of the neo-Tethys (Adamia et al. 2011; Kazmin, Schreider, and Bulychev 2000). This inversion produced the fold and thrust belts of the Caucasus Mountains, associated with the foreland Kura Basin (Fig. 1b). The Kura fold-thrust belt initiated during the Pliocene-Pleistocene, although exact timing and evolution remains not fully resolved (Forte et al. 2014).

The Kura Basin is infilled with sedimentary successions up to 13 km-thick in its depocenter (Abdullayev et al. 2012; Brunet et al. 2003) and up to 3 km-thick along its margins (Lazarev et al. 2019; van Baak et al. 2013; Forte et al. 2015). Throughout the different regional stages, this Kura Basin embayment was repeatedly flooded during Caspian Sea highstands and emerged during lowstands. The Pliocene-Pleistocene Akchagylian regional stage represents mainly mudstones in its deepest parts (Lazarev et al. 2019) and continental deposits with terrestrial mammal bones in its western extremity (Agustì et al. 2009). The major Caspian Sea transgression appears therefore to have been limited to some extent in the marginal basin. A study by Forte et al. (2014) on interior Kura Basin sediments found evidence for a diachronous nature of Akchagylian deposits and a younging of the transgressive sediments towards the west of the Kura Basin, related to the initiation of the Kura fold-thrust belt. Thereafter, the Early Pleistocene Apsheronian regional stage is marked in the Kura Basin centre by alternating offshore mudstones, coastal sandstones, and terrestrial mudstones enriched in brackish and freshwater fauna (Lazarev et al. 2019; Jorissen et al. 2019). These conditions highlight shallower environmental settings compared to the Caspian Sea.

2.1. The Kvabebi section

The Kvabebi section crops out on a hillside near the Iori River, 17 km southwest from the hamlet of Kvemo Bodbe in the Kakheti region of Eastern Georgia (Fig. 1b). The section starts at the easternmost hillside near N°41'45.58", E°45'71.40" and stratigraphy can be followed westward along the foothill until N°41'45.65", E°45'71.27". The studied interval is situated along the northern limb of a 15° plunging anticline towards 300° (WNW), bounded to the north by a small sub-vertical ENE-WSW trending fault. The section has previously been described and logged in low resolution by Agustì et al. (2009) and Ali-Zade et al. (1972) mainly for the purpose of biostratigraphy, since the section records abundant mammal bones. Geological maps from Bairamov et al. (2008) suggests that the Kvabebi section covers the Akchagylian and Apsheronian regional stages and paleomagnetic data suggest an age between approximately 3.3 and 2.1 Ma (Agustì et al. 2009). Estimated thicknesses for this section range from 170 to 350 m. The lower part of the section (0-130 m) comprises a succession of brownish or bluish laminated mudstones with marine to brackish-water molluscs. The middle part of the section (130-225 m) shows a transition to sand-dominated deposits and the disappearance of marine mollusc fauna. The upper part (225-280 m) contains reddish-brown mudstones, sandstones, and conglomerates with very sparse freshwater fauna. This succession is believed to represent a general regressive trend from Akchagylian brackish water nearshore deposits to Apsheronian freshwater fluvial deposits (Agusti et al. 2009).

2.2. The Kushkuna section

The Kushkuna section is situated 20 km north of the town Aghstafa in western Azerbaijan (Fig. 1b). The section starts near a sand quarry at N°41'28.94", E°45'46.91" and continues westward through several canyons upslope to the hilltop at N°41'29.99", E°45'48.01". The section runs near the hinge of an ENE gentle plunging anticline oriented 073°. Geological map from Bairamov et al. (2008) similarly suggests that the Kushkuna section covers the Akchagylian and Apsheronian regional stages along a 300 m thick succession. The base of the section (0-40m) is of unknown age and consists of obliquely laminated tuffogene sandstone bearing volcanic glass. The lower part of the section (40-120 m) mostly consists of dark-grey mudstones enriched in brackish water molluscs, with some horizons made of dark-brown organic-rich mudstones with freshwater molluscs. Thereafter, the section records sandstones (120-162 m) and dark-grey and dark-brown mudstones (162-205 m) bearing abundant brackish and freshwater molluscs. Upwards in the section (205-222 m), a sandy interval occurs that is devoid of mollusc fauna with a rich assemblage of mammal bones. The transition to the upper part of the section, the presumed Apsheronian (222-300 m) is marked by alternating sandy-gravel deposits and yellowish-grey and reddish-grey mudstones without any fauna. This succession is interpreted as a general regressive trend from Akchagylian marine to nearshore to Apsheronian freshwater environments (Ali-Zade et al. 1972).

3. Methods

3.1. Facies analysis

In order to propose a more detailed environmental and climat-

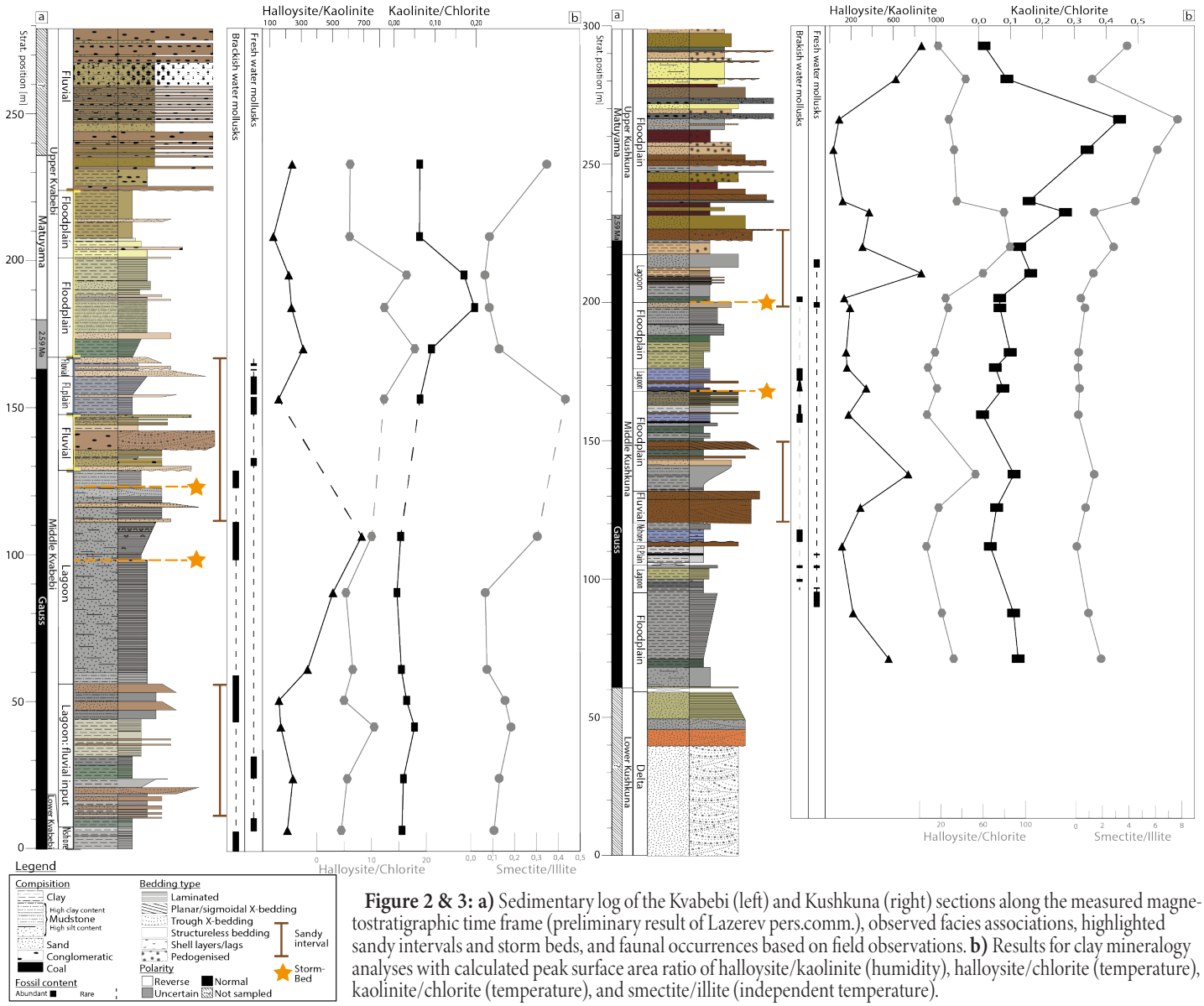

Figure 2 & 3: a) Sedimentary log of the Kvabebi (left) and Kushkuna (right) sections along the measured magnetostratigraphic time frame (preliminary result of Lazerev pers.comm.), observed facies associations, highlighted sandy intervals and storm beds, and faunal occurrences based on field observations. **b)** Results for clay mineralogy analyses with calculated peak surface area ratio of halloysite/kaolinite (humidity), halloysite/chlorite (temperature), kaolinite/chlorite (temperature), and smectite/illite (independent temperature).

ic reconstruction of the Kvabebi and Kushkuna sections, the two sedimentary successions were logged 1:250 with a resolution of 0.25 meter using a 1.5 m Jacob's staff. The thinnest stratigraphic unit examined was 5 cm thick. Based on detailed logging, the Kvabebi section is measured to be around 280 m-thick and the Kushkuna section around 300 m-thick (Fig. 2a, 3a), which corrects the previous estimations (Agustì et al. 2009; Ali-Zade et al. 1972).

Changes in lithology, colour, grain sizes, sedimentary structures, contact with adjacent beds, and faunal assemblages were recorded in detail. By comparing these field observations with well-established classification schemes (Miall 2006; Postma 1990), fourteen lithofacies are described and interpreted in context of their depositional processes (Table 1). These lithofacies are grouped within five distinct facies associations specific for different depositional environments. Crude determination of mollusc fossils in the field allowed for preliminary interpretation of depositional conditions and preferred salinities. Paired shells are thought to be deposited in situ, while fragmented and abraded shells are thought to be reworked.

Paleocurrent directions were measured where possible on 3D cross-bedding, scour marks, and pebble imbrication with a geological compass and corrected for set-boundary or bedding plane orientation. Bedding planes and paleocurrent indicators are first corrected for the fold axis plunge, before correcting the paleocurrent indicators for bedding plane tilt. Statistical analysis of their distribution is presented in equal-area rose diagrams (Nemec 1988) with 30° bin size.

3.2. Grain size analysis

A total of 31 sediment samples were taken at some of the most representative lithologies in both sections to later be analysed for grain-size distribution, in order to better characterise sedimentary processes present in each facies association. Grain-size analyses were executed on the sample siliciclastic fraction in a laser particle sizer, Mastersizer 2000, in the Comparative Sedimentology Laboratory, Department of Earth Sciences, Utrecht University. To obtain the insoluble residue, about 1 g of sample was placed in 50 mL centrifuge tubes and treated with a 0.3M CH3COOH solution to remove carbonate according to Ostrom (1961) and organic matter was removed using Sodium Hypochlorite according to Mikutta et al. (2005).

To proceed with grain-size measurement with the laser particle sizer Mastersizer 2000, the solution was transferred to the sample dispersion unit (Hydro 2000G) of the instrument to be diluted until a laser obscuration of 20±5% was reached. Dispersion of the

Table 1: *Lithofacies description and interpreted sedimentary process for the Kvabebi and Kushkuna sections.*

Code	Grainsize	Structures	Inclusions	Processes	Nearshore	Lagoon	Floodplain	Delta	Fluvial
Gh	Pebbles	Horizontally stratified gravel (0.5-2m), imbrication	-	Traction flow, longitudinal bedform, lag deposit					■
Gc	Pebbles	Trough and sigmoidal cross bedded 0.5m, erosive base, possible fining up	-	Traction flow, minor channel fill					■
Sh	Silt-coarse sand	Horizontally laminated (1-10mm) silt and sand, possible reverse grading, possible erosive at base	Oxidized organic material, possible volcanic glass, possible roots	Plane bed flow regime or suspension settling			■	■	
St	Fine sand-coarse sand	Trough cross-bedded (0.1-2m), often normal graded, possible broad shallow scours (1-10m), possibly channelized	Possible clay pebbles, possible shell fragments, possible organic material	Migration of 2D/3D sinuously crested dunes		■	■	■	■
Sc	Medium-coarse sand	Tabular or sigmoidal cross-bedded (0.1-0.5m), possible lateral accreting cross-beds	Possible clay lenses, possible clay pebbles, organic material	Migration of 2D crested dunes			■	■	■
Sm	Very fine sand-coarse sand	Structureless	Possible shell fragments (mm-scale), possible roots	Rapid suspension fall-out or structuration destroyed by intense bio-reworking		■	■		
Fg	Mudstone	Lenses (0.2 m thick) of pebbles	-	-					■
Fsl	Clay	Laminated (1-5mm) alternations of clay and oxidized silt. Clay dominant	Possible shell layers, shell fragments, possible organic material, possible roots	Suspension settling in restricted area		■			
Fsm	Clay-medium silt	Structureless	Large organic material, leaf imprints, possible flat gastropods, possible slickensides, possible shell fragments, roots	Suspension settling in restricted area		■	■		
Fl	Mudstone	Mudstone, may be laminated (1-5mm)	Concentrated shell layers/lags with mixed brackish (in situ) and fresh water fauna	Suspension settling in open area with occasional storm transport	■				
Fr	Mudstone	Mudstone with oxidized sand/silt horizontal laminations (1-5mm)	Rare bones, possible mottled, possible flat gastropods, slickensides, organic material, roots	Suspension settling in swampy environments, pedogenesis			■		
C	Clay-fine sand	Structureless	Very rich in organic material, leaf imprints, possible mottling, possible small entire shells, roots	Suspension settling in swampy environments			■		
P	Clay-silt	Crumbly texture	Rodent tooth, remineralized roots, possible calcrete horizons, slickensides, organic material	Soil formation			■		

samples was ensured by adding 25 mL of a dispersing solution (44.6 g Na4P2O7•10H2O and 4.24 g Na2CO3 in 1 L deionized H2O) and by ultrasonication (maximum tip displacement of 4 µm) for exactly 1 minute prior to starting the measurement. The frequency of grain size was recorded from 0.02 to 2000 µm divided logarithmically in 100 class intervals. Values of 1.544 and 0.9 were used for the refractive and absorption indices of the samples, respectively. The residual was always less than 1.6 %. Duplo samples were prepared and an average difference of <5% was obtained.

Grain-size distribution in sedimentary lithofacies reflects characteristic depositional processes (McLaren and Bowles 1985; Folk 1966; Sun et al. 2002) that may help to better characterise each facies association developed in Section 3.1. Results were converted from µm to φ-scale (Krumbein 1936). The statistical moments method was used to obtain values for the mean grain-size, skewness, and kurtosis of the distribution and sorting (Krumbein 1936, 1955). An effective method to determine the general mode of transport is to analyse the relation of the grain-size median (d50) with the one percentile (d99) (grain size of the coarsest one percent of grains). This relation is projected in a C-M plot (Passega 1964) that enables simple categorization of lithofacies based on their dominant transport mode. The cumulative grain-size distribution is plotted on a probability density scale to emphasize the tails of the distribution. Interpretation of specific processes belonging to populations in these graphs was originally developed by Vischer (1969) mainly for deltaic and beach sediments, and is here adapted where suitable and expanded upon where it was underdeveloped for detailed fluvial concepts. The Vischer graphs in this research work display only the trend of grain-size populations, not the individual datapoints, for the sake of clarity. The most typical curve of each lithofacies was selected to highlight the most representative processes occurring in each facies association. The original figures can be found in Appendix A.

3.3. Clay mineralogy

A total of 48 sediment samples were prepared along both sections and analysed for their mineralogic composition. The mineralogic composition of the bulk composition and insoluble clay fraction (≤2 and ≤10 µm) was determined by X-ray diffractometry (XRD (Moore & Reynolds 1989; Brindley &Brown 1980; Brown 1980)

Firstly, the bulk mineralogical composition of 38 samples throughout both sections was determined. Samples were ground in an agate mortar until they had the texture of flour to ensure homogeneity and a statistically relevant number of grains that contributes to the signal. The powders were mounted in 25 mm disc with a sample thickness of 1 mm.

Secondly, to identify specific clay mineral signals, oriented clay mounts were prepared for 10 samples of different lithofacies types. Oriented samples were prepared by splitting the clay fraction (<2 and <10 µm) from the insoluble residue suspension that was inherited from the procedure in the grain-size section. Five millilitres of a dispersing solution (44.6 g Na4P2O7•10H2O and 4.24 g Na2CO3 in 1 L deionized H2O) were added to the samples before centrifuging to seperate the clay fraction from coarser particles using a modified form of Stokes's law (Svedberg and Nichols 1923). The clay suspensions were rinsed three times with deionized water to remove the dispersing agentand split into two centrifuge tubes. A 1 M KCl solution was added to one and a 0.1 M MgCl2 solution to the other. The clay minerals

were separated from the solution three times and, each time, the solution was replaced with fresh solution. The saturated clay suspensions were rinsed three times with deionized water. To allow for quantitative analysis, the samples where freeze-dried, weighed, and diluted with deionized water until a concentrated suspension of exactly 60 mg/mL was achieved. About 1 mL of sample was distributed on glass microscope slides, which were previously cleaned with ethanol, using a pipette. All slides were allowed to air-dry at room temperature, partly in a desiccator, and then analysed in air-dried state. The Mg-saturated slides were then exposed to the vapour of ethylene-glycol in a dish with a lid in a 60°C oven for at least 12 hours and analysed immediately after leaving the oven (Bradley 1945). The samples did not come in contact with the liquid glycol. The K-saturated slides were gradually heated up to 550°C in a furnace and remained at that temperature for at least 8 hours. They were analysed after cooling to room temperature in a desiccator.

For both the bulk and clay mounts analyses, samples were measured using a Bruker d8 Advance diffractometer (Cu Kα, 40 kV, 40 mA). Scanning range was from 3 to 70 °2θ. The stepsize and measuring time per step varied from sample to sample, in order to achieve the highest quality XRD trace. The divergence slit moved mechanically and automatically so that a fixed sample illumination was secured. Soller slits were not used and an automatic air-scatter knife was employed. Random powder samples were measured on a rotating platform revolving at 15 RPM, to further increase the number of grains that contribute to the measured pattern. Oriented clay mounts were measured on a stationary platform. XRD-patterns that were obtained by both methods, the diffrac.eva software was used to strip the Kα2 and remove the background signal. Peak surface area and peak height were calculated using this software. The analytical precision is estimated to be 10-15 %. The peaks used for these ratios are (in d-spacing): chlorite 3.54 Å, kaolinite 3.58 Å, halloysite 4.49 Å, chlorite 4.72 Å. For the smectite/illite ratio the height of the smectite dome between 10-15 Å and the height of the illite peak at 9.9 Å are used, to provide a ratio that is independent of chlorite. Distinguishing smectite and smectite mixed layers is based on the air-dried/E.G.-solvated analysis on selected oriented clay mounts, and assumed to be applicable on random powder patterns. The same is applied for distinguishing chlorite from kaolinite, based on air-dried/550°C.

4. Results

4.1. Environmental reconstruction

In order to reconstruct the paleo-environmental conditions in the western Kura Basin, depositional environments are identified and characterised using facies associations. Changes in depositional environments over time allow for reconstruction of the sedimentary history of the basin.

4.1.1. Depositional environments

Lithofacies types are related to specific depositional processes and therefore occur together. Facies associations help to group lithofacies types and infer the depositional environment.

4.1.1.1. Nearshore facies association

Sedimentary description: The first facies association consists of a 5 to 10 m-thick interval made of light-grey mudstones that may be massive or laminated (Fl) (Fig. 4l). Laminations are made of 1 to 5 mm-thick silt-laminae. Sediments contain in situ dispersed mollusc fauna (Fig. 5) and occasionally cm-thick layers or lags, comprising marine to freshwater reworked mollusc fauna (Fig. 5, 6).

Grainsize analysis: Nearshore deposits, associated to lithofacies Fl, tend to have small (<10 µm) median (d50) grain-size but high (>1 mm) coarsest (d99) grain-size (Fig. 7). The grain-size distribution (Appendix A) shows a gap from 1 to 5 φ, with one peak between 0 and -1 φ. On the CM diagram, this lithofacies is plotting in the 'mixed processes' region (Fig. 7). Mixed processes represent a combination of maximum and median grain-size that cannot be attributed to a single mode of sedimentary transport.

Two populations both finer than 4 φ are evident in the cumulative grainsize distribution (Fig. 8b). The predominant population is representative for suspension settling is responsible for 75-90% volume of the grains, occurs finer than 5 φ and presents a relatively low gradient. Suspension settling appears to be the dominant processes, although the sorting is poor. The population associated with grain suspension (5 - 4 φ) is only responsible for 10-25% volume of the grains, plotting on a relatively high gradient. Grain suspension is rather limited but represents good sorting of few disperse coarse grains mixed in with the rest of the volume in the sediment.

Interpretation: This facies association displays very low to low depositional energies, occasionally alternating with medium depositional energies . Overall silt to clay particle size constituting this mud dominated interval implies suspension settling as dominant sedimentary process, as confirmed by a large suspension settling contribution in the grainsize distribution. A small component of grain suspension indicates that disperse coarser grains are mixed in with the rest of the sediment, potentially originating from a local river. Laminations of silt comprised within the mudstones express increased distal river discharge, which may be seasonal. The in situ marine to brackish water mollusc fauna indicate increased salinities. Occasional storm-transport may provide a mixture between brackish and freshwater mollusc fauna, reworked from more coastal regions. This first facies association is consequently interpreted as a nearshore environment.

4.1.1.2. Lagoon facies association

Sedimentary description: The second facies association varies in thickness from 7 to 70 m. It chiefly consists of grey mudstones that are massive (Fsm) or laminated (Fsl) (Fig. 4j). Laminations are made of 1 to 5 mm-thick silt-laminae. Storm vortex wave ripples of fine sand occur very rarely in mudstone. Sediments may contain cm-scale terrestrial organic material. The massive mudstones may show signs of cm-scale vertical plant roots. Fragmented brackish water mollusc fauna occurs concentrated in <1 cm-thick layers or lags (Fig. 5). Non-fragmented freshwater molluscs, like Unio or Planorbis (Fig. 6), typically occur in situ dispersed in the sediment. Mudstones irregularly alternate with meter-scale layers of structureless sandstones (Sm) (Fig. 4g) or cross-bedded sandstones (St) with preserved cross-set thickness of 0.1 to 2 m (Fig. 4e). Sandstone beds display both normal and reverse grading.

Grainsize analysis: Lagoon deposits, represented by lithofacies Fsl, Fsm, Sm, and St, show great variety in sedimentary processes. The different lithofacies cover in fact most of the CM

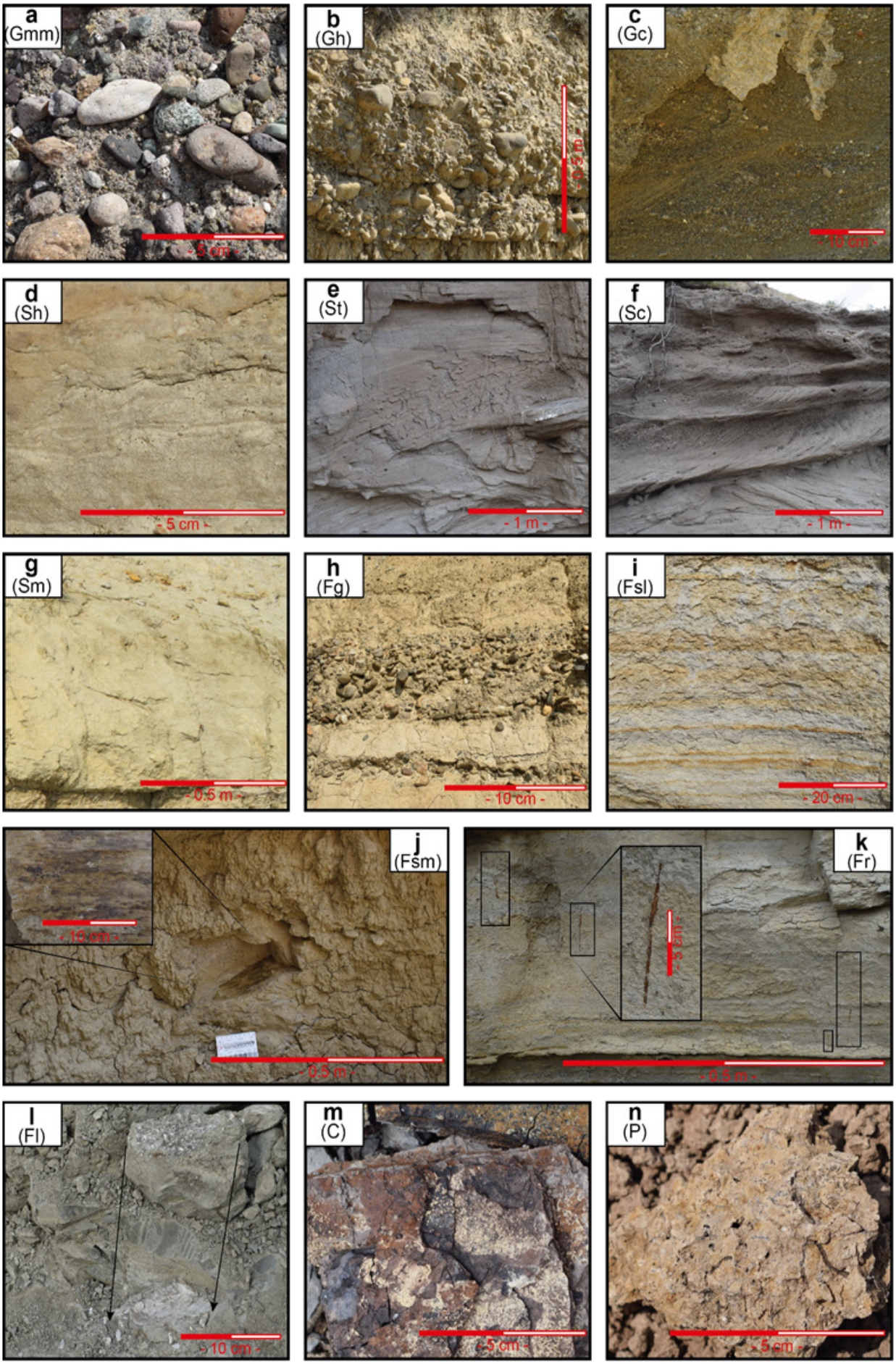

Figure 4: Annotated field pictures of the different lithofacies identified along the section. Letter coded correspond to lithological description in Table 1. Gravel (Gmm, Gh, Gc, Fg) clast composition is different for each section; Kushkuna exhibits a wider variety of colour and minerals with a volcanoclastic signature, Kvabebi is more uniform and richer in lithoclasts and metasediments. The same is true for sandy lithofacies (Sh, St, Sc, Sm). Fine-grained lithofacies (Fsl, Fsm, Fr, Fl, P) might be laminated (i) or show varying degrees of soil formation like slickensides (j), roots (k), or calcretisation (n). The most marine faunal assemblage is found in lithofacies Fl.

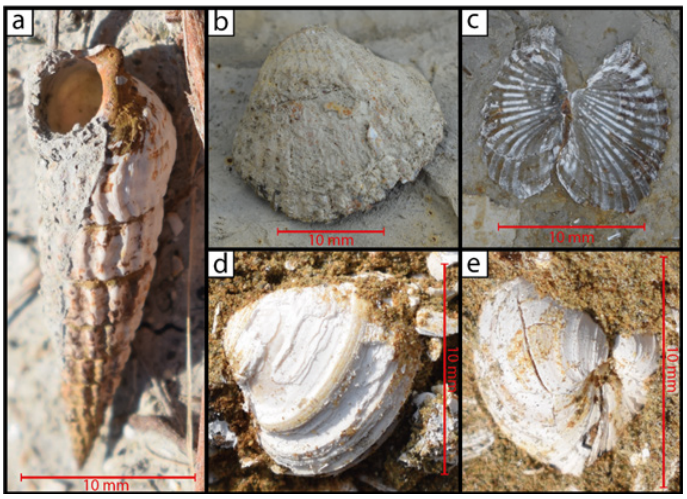

Figure 5: Field pictures of Akchagylian mollusc species present in the Kvabebi and Kushkuna sections and indicative of brackish water conditions: **a)** *Piranella sp.*, **b)** *Cardium sp.*, **c)** *in situ* paired *Cardium sp.*, **d)** *Avimactra sp.*, **e)** *in situ* paired *Avimactra sp.*

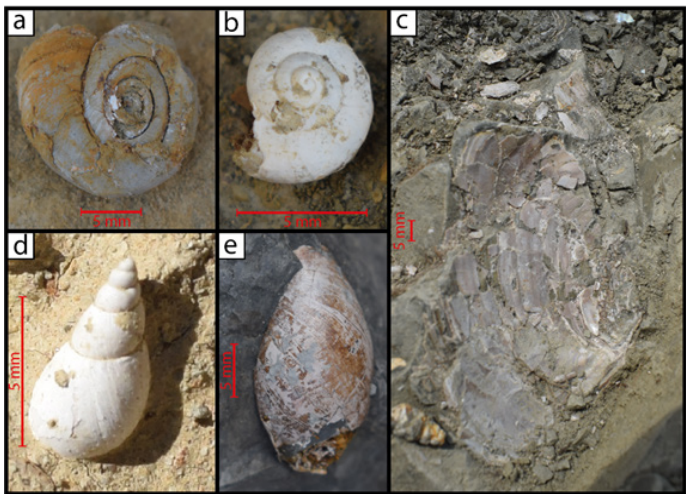

Figure 6: Field pictures of Akchagylian mollusc species present in the Kvabebi and Kushkuna sections and indicative of freshwater conditions: **a,b)** *Planorbis sp.*, **c)** *Unio sp.*, **d)** *Clessiniola sp.*, **e)** *Melanopsis sp.*

diagram (Fig. 7). Fsl lithofacies plot in both the 'suspension settling' and the 'graded suspension' regions. Fsm lithofacies plot in the 'mixed processes', and 'uniform suspension' and 'graded suspension' regions. The Sm lithofacies plot in both the 'graded suspension' and the 'mixed processes' regions.

Suspension settling corresponds to both small median and coarsest grain-size and is dominant in a protected or standing body of water. Graded and uniform suspensions represent grain transport in a flowing body of water. Graded suspension occurs when median and maximum grain-size are decreasing when the distance from the bed increases. At the point where the concentration and maximum grain size become relatively constant, the suspension is called uniform.

This variety of processes is also evident from the cumulative grainsize (Fig. 8c). General grain-size distribution presents coarser grain-sizes up to 1 φ. Lithofacies Fsl shows one population in the suspension settling domain (>4 φ), making up more than 95% volume of grains with a poor to moderate sorting. The fine-grained lithofacies Fsm shows very good sorting in the saltation fraction (1-4 φ) that deposited 90% volume of grains. The remaining 10% volume is moderately sorted and deposited by grain suspension (4-5 φ). This lithofacies deposited as the result of high energy flow and rapid sedimentation. The Sm lithology shows a moderately sorted saltation population (1-4.5 φ) making up 50% volume of sediment. The fine-grained tail is very poorly sorted but abundant.

Interpretation: This facies association highlights very low to low depositional energies alternating with medium depositional energies. Mud-dominated sedimentation is mainly from suspension in a restricted environment, with very rarely indication of storm surges in storm vortex ripples (Bagnold 1946). The rapid and high-energy deposition of lithofacies Fsm as indicated by the grainsize distribution indicate storm washover processes. The grainsize distribution of massive sands (Sm) does not confer to simple sedimentary processes, and the absence of lamination may therefore be due to (bio-)reworking of the sediment. Cross-bedded sand bodies infer increased sediment supply caused by migration of channels or increased discharge of a nearby river system. Inverse grading in sand may indicate migration or progradation of subaqueous dunes. Freshwater mollusc species indicate a nearby source of freshwater, while fragmented brackish water fauna may be deposited in layers or lags during storm events. Identified storm beds are indicated in Fig. 2 and 3. Roots and terrestrial plant remains indicate a protected system close to land. These characteristics lead to the interpretation of a highly dynamic lagoonal environment for this facies association with a vegetated coast, freshwater, and sediment input from a nearby river and occasional storm surges.

4.1.1.3. Floodplain facies association

Sedimentary description: The third association is the most diverse in lithofacies. It consists in a 10 to 80 m-thick interval dominated by grey mudstones with intermittent sandstone beds. Blue to green mudstones occur in 5 to 20 m-thick intervals. Mudstones are structureless (Fsm) (Fig. 4j) or laminated with 1 to 5 mm-thick silt-laminae (Fr) (Fig. 4k). Deposits may be rooted and may contain slickensides. Some horizons contain remineralised roots or calcrete horizons (P). Some mudstones are extremely rich in cm-scale terrestrial organic material deposited in <20 cm-thick dark coloured beds (C) (Fig. 4m). Brown fine to very coarse sandstones occur in <2 m-thick beds and may be structureless (Sm) (Fig. 4g), horizontally laminated with 1 to 10 mm-thick silt laminae (Sh) (Fig. 4d), trough cross-bedded with preserved cross-set thickness of 0.1 to 2 m (St) (Fig. 4e) or tabular cross-bedded with preserved cross-set thickness of 0.1 to 0.5 m (Sc) (Fig. 4f). Sandstones contain mm-scale terrestrial organic material and very rarely unidentified mammal bone fragments. Some cross-bedded sands are erosive and contain cm-scale clay pebbles in 10 to 20 cm-thick lag deposits at the base. Paleocurrent measurements of these sandstones indicate non-uniform transport directions generally to the SW (see Fig. 9f). Structureless or horizontally laminated sands may have cm-scale vertical roots.

Grainsize analysis: Floodplain deposits, comprising lithofacies Fr, Fsm, Sm, Sc, St, Sh, C, and P, show a large spread between mud-dominated and sand-dominated lithologies (Fig. 7). Muddy lithofacies mostly plot in the 'suspension settling' and 'uniform suspension' regions, while sandy lithofacies mostly plot in the 'bedload' and 'mixed processes' regions. The bedload region reflects the coarsest median and coarsest grain-sizes. Transport is through rolling of grains, indicating an environment with

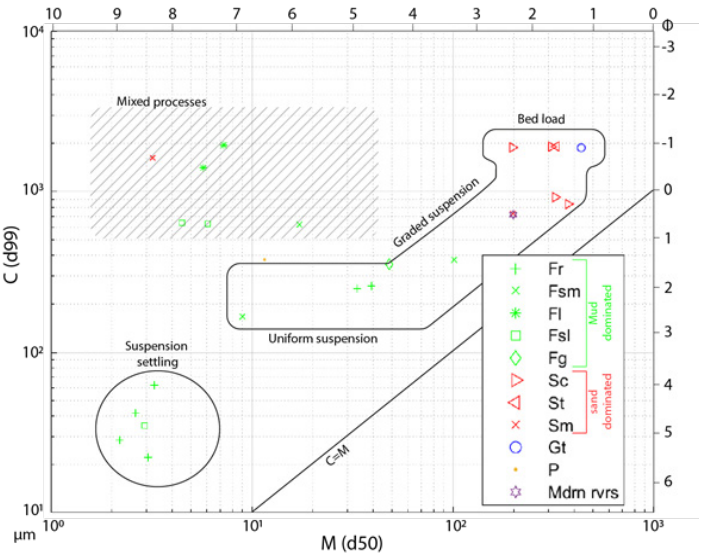

Figure 7: Observed lithofacies plotted in the different contouring boxes of the Passega diagram (1964), corresponding to specific sediment transport modes. The axes represent the median on the horizontal axis and coarsest fraction on the vertical axis, with the coarsest combination in the upper right and the finest in the lower left of the diagram. The 'mixed processes' region represents a combination of grain sizes that cannot be attributed to a single depositional process, and are likely the result of processes like bioturbation, winnowing or flushing.

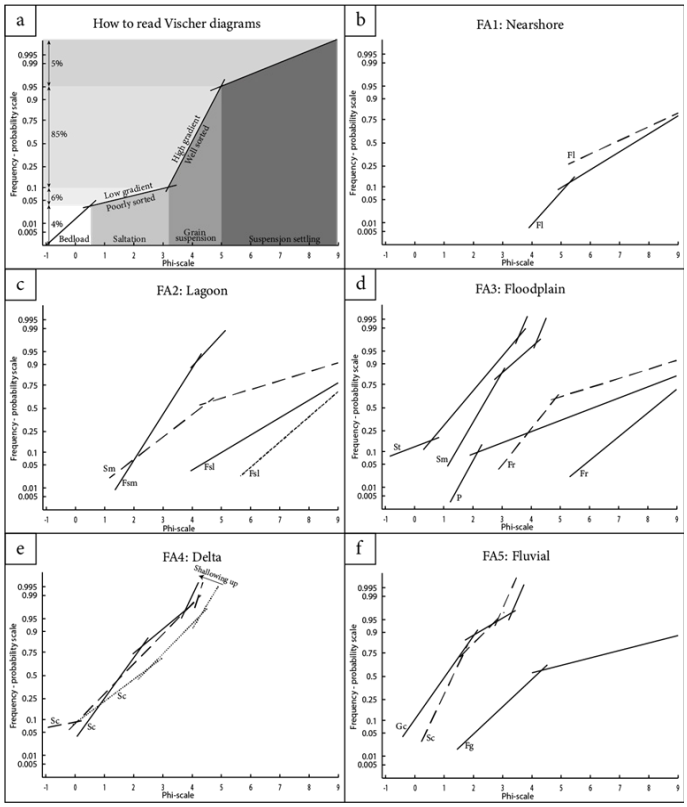

Figure 8: Cumulative grainsize distribution on a probability density frequency axis as introduced by Vischer (1969) per facies association: **a)** Explanations how to read the Vischer diagrams, **b)** nearshore environments, **c)** lagoon environments, **d)** floodplain environments, **e)** deltaic environments and **f)** fluvial environments. The finest grained lithofacies are in nearshore environments and the coarsest are in deltaic and fluvial environments. Floodplain deposits are the most variable.

enough energy to transport sand grains or pebbles as bedload in a traction flow (Sohn 1997; Todd 1989). The structureless sandstone (Sm) plots in the unconformable area.

More detailed analysis of the texture of floodplain deposits confirms this high variety in sedimentary styles (Fig. 8d). The coarsest grain-size in these sediments is -1 φ. The finest lithofacies is Fr and presents two types of curves. The solid line has one suspension settling fraction (>5 φ) up to 99% volume. This facies is deposited in nearly stagnant water. The well sorted saltation population (3-4.5 φ) in the dashed curve of lithofacies Fr makes up 50% by volume while the grain suspension fraction (>4.5 φ) is moderately sorted and makes up the other 50%. The lithofacies P that shows signs of pedogenesis displays a minor but very well sorted saltation population (1-2 φ) that deposited less than 10% volume. The other 90% volume is one very poorly sorted population finer than 2 φ. The sand-dominated lithofacies Sm shows three populations in total. Two saltation populations (1-4 φ) together making up 95% of the sediment volume are both well-sorted. The coarser saltation population is better sorted than the finer saltation population, indicating that the primary current velocity was able to sort the coarser fraction along the flow bed, while finer particles get entrapped without much preference. This distribution shows typical graded suspension deposition. A very well-sorted grain suspension population forms the other 5%. The coarsest lithofacies St also shows three different populations. The coarsest represents a bedload population (-1-0.5 φ) for over 10% volume. The two other populations representing 90% of the sediment volume are well-sorted, not finer than 3.5 φ and deposited by grain saltation. This cross-bedded sandstone was deposited by traction flow.

Interpretation: This facies association displays a fluctuation between very low to low depositional energies with medium depositional energies. Most fine-grained sediments are interpreted as overbank deposits. The grainsize distributions of the finest-grained lithology Fr point at distal overbank flow (dashed Fr curve) as the responsible transport mechanism reaching the fully stagnant aquatic environment (solid Fr curve). Roots indicate that vegetation was established during more quiet intervals. Slickensides in these mudstones indicate seasonal wetting and drying (Kraus and Hasiotis 2006; Gray and Nickelsen 1989), and extensive accumulation of organic material is facilitated by submergence of the land (C). More extensive soil formation in lithofacies P flushed al grains finer than 2 φ leaving a very well sorted framework of grains in the 1-2 φ range. The pore-space was subsequently filled by leached finer grained sediments and cement without sorting. The typical graded suspension distribution of lithofacies Sm is characteristic for proximal overbank sediments that are deposited rapidly. The cross-bedded sandstone (St) that is deposited through traction flow records channelized transport (O'Brien and Wells 1986) in non-uniform directions (Fig. 9f). Clay pebbles in these deposits represent the ripping up of the overbank structure, altogether leading to the identification of crevasse-splay events. This facies association records suspension settling in swamps or other stagnant bodies of water, distal and proximal overbank deposits, soil flushing, and channelized transport. This generally quiet but episodically rather dynamic depositional setting is therefore interpreted as a floodplain environment. It is noteworthy that all mammal bone remains were found in this floodplain facies association, in coarse-grained deposits.

4.1.1.4. Delta facies association

Sedimentary description: Only present in the base of the Kushkuna section, this fourth facies association represents

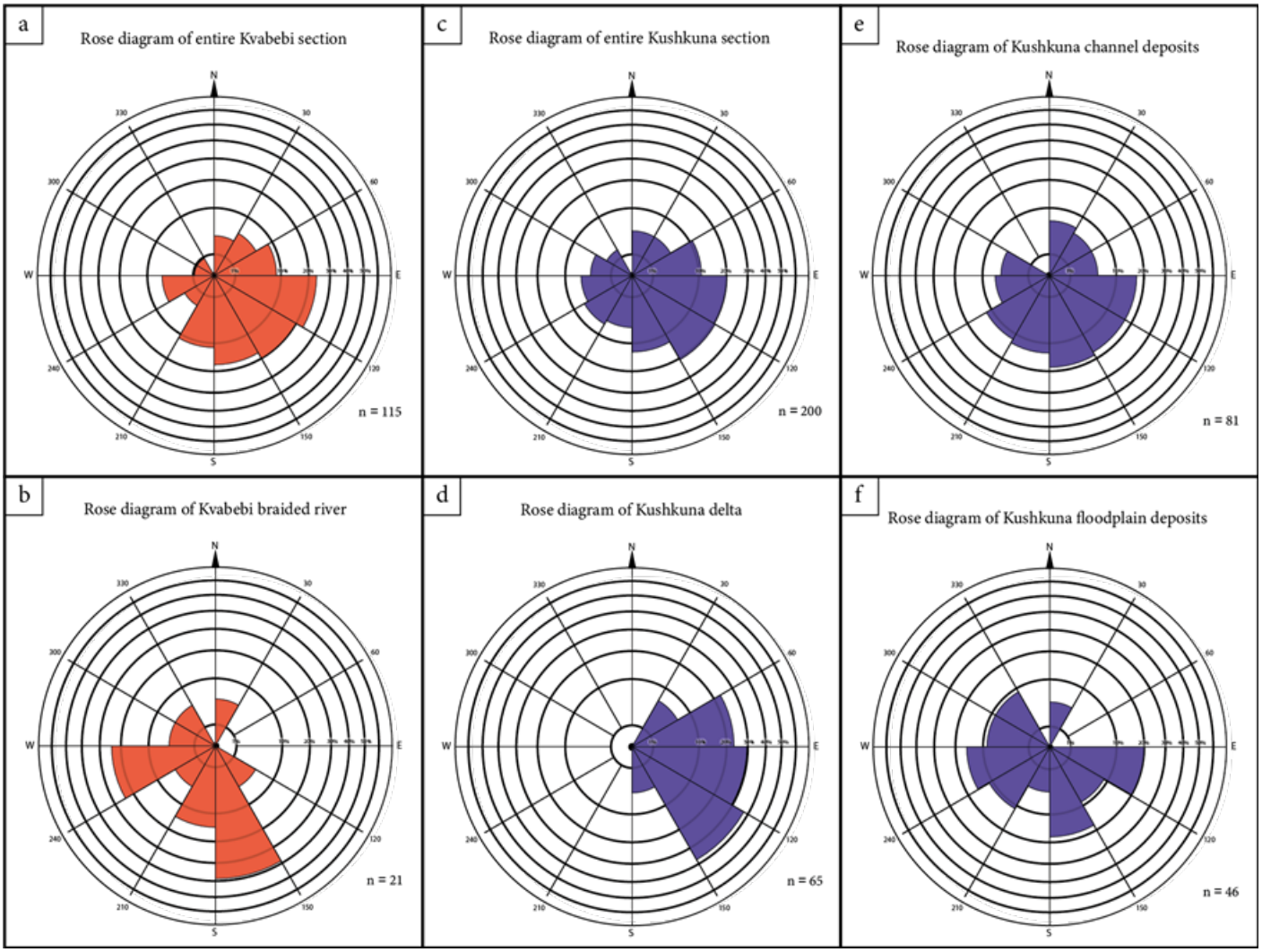

Figure 9. Paleocurrent measurement indicating south-east transport directions for the two sections. The Kvabebi braided river indicates transport directions towards the south. The Kushkuna delta shows transport directions towards the south-east.

at least a 60 m-thick interval dominated by white sandstones enriched in volcanoclastic material, overlain by orange-grey sandstones and covered by grey organic rich sandstones enriched in volcanic glass. Differently coloured units are bound by sharp or erosional surfaces. The two first types of sandstones are characterised by meters-thick beds of fine to medium sediments with meter(s)-scale structures. Trough cross-bedding with preserved cross-set thickness of 0.1 to 2 m (St) (Fig. 4e), as well as tabular and sigmoidal cross bedding with preserved cross-set thickness of 0.1 to 0.5 m (Sc) (Fig. 4f) are prevalent in these sandstones. Meter(s)-scale slump structures are present at the base of the white interval. Terrigenous cm-scale pebbles form <5 cm-thick lag deposits. White clay rip-up clasts up to 20 dm may be non-continuously distributed at the bottom of cross-beds. The third type of sediments found at the top of this facies association is marked by fining up sandstones with 1 to 10 mm-thick silt laminations (Sh) (Fig. 4d). These finer sediments contain dm-scale channel fill structures and are enriched in cm-scale terrestrial organic material. Paleocurrent measurements in this sand-dominated facies association indicate direction of transport towards ESE (Fig. 9d).

Grainsize analysis: Delta deposits, associated with lithofacies Sc, St, and Sh plot in the 'bed load' region (Fig. 7). Energy was very high with a mode of transport mainly dominated by saltation and rolling of grains, while the finer fraction was winnowed.

Delta lithofacies grainsize distributions are represented by three different curves, which after careful inspection show subtle differences in sedimentary processes (Fig. 8e). Sandstones show a grain-size range from -1-0 to 5 φ and saltation populations that make up 90% of the sediment volume. The finely-dotted curve represents the lowermost white sandstone of the delta and shows one finer saltation population (0-2.5 φ) that is better sorted than another coarser saltation population (2.5-4 φ). The dashed curve represents the orange-grey sandstone overlying the previous sandstone and indicates poorly sorted bedload (-1-0 φ) sedimentation along only one well-sorted saltation population (0-4 φ). The solid line denotes the uppermost grey sandstone of the delta, showing three populations similarly distributed as the dotted curve. A bedload population is absent and the coarser saltation population (0-2 φ) is better sorted compared to the finer saltation population (2-4 φ).

Interpretation: Medium to high depositional energies are highlighted in this fourth facies association. Succession of large-scale trough and planar cross-beds that may be slumped, suggesting slope instability due to great volumes of sediment filling up a large accommodation space. The grainsize distribution of the white sandstone at the base indicates winnowing of the finer saltation population by a secondary current, a process that takes place near the shore (Visher 1969). Above a grain-size of 2.5φ, this secondary current is not able to transport grains. Erosional

surfaces are indicative of channel migration, a process that is confirmed by the channelized flow environment indicated for the orange-grey sandstone due to its well-sorted saltation population. For the uppermost grey sandstone, a stronger current was able to winnow the coarser fraction and later trapped finer particles in the pores. The shallower part of a channel represents these conditions. This facies association thus represents sedimentation in a highly energetic environment with channelized flow and secondary currents. The scale of the sedimentary structures and the univalent paleocurrent directions (Fig. 9d) allows for the interpretation of a deltaic system prograding towards the east. The small-scale channel fill structures in the fining-up sandstone at the top of the association indicate the lower energy delta-top.

4.1.1.5. Fluvial facies association

Sedimentary description: The fifth association is made of a 7 to 50 m-thick interval dominated by brown conglomerates and coarse-grained sandstones deposited in meter(s)-thick beds. Conglomerates display horizontal bedding with possible dm-scale imbricated terrigenous pebbles (Gh) (Fig. 4b) or dm-scale cross-beds with preserved thickness up to 0.5 m (Gc) (Fig. 4c). Conglomeratic beds may show an erosive base. Medium to very coarse sandstones are trough cross-bedded with preserved thickness of 0.1 to 2m (St) (Fig. 4e). Mudstones with cm-scale terrigenous pebbles deposited in dm-thick layers (Fg) (Fig. 4h) are found interbedded with the conglomerate and sandstones beds. The pebbles present similar composition as the underlying coarser deposits. This facies association is dominant in the top of the Kvabebi section, where it is coarsening up in 2 to 3 sequences of 15 to 35 m-thick, where pebble imbrication shows general transport towards the south (Fig. 9b).

Grainsize analysis: Coarse fluvial deposits, embodying lithofacies St, Sc, Gc, and Gh plot in the 'bed load' region and mud-dominated facies Fg plots in the 'graded suspension' region (Fig. 7).

These lithofacies show fine-grained sediments as well as coarse sizes up to -0.5 φ (Fig. 8f). The fine-grained lithofacies Fg demonstrates a moderately sorted saltation population (1-4 φ) that makes up 50% volume of sediment. The other volume half is a single very poorly sorted population of fine-grained material (>4 φ). The sand and gravel dominated lithofacies Sc and Gc show dominantly bedload transport (<1.5 φ), making up more than 75% of sediment volume. The saltation populations (1.5-3 φ) constitute less than 25% volume of the sediment and are moderately sorted.

Interpretation: These deposits are dominated by high to very-high transport energy. The finer-grained mudstones Fg display grain saltation and graded suspension that may be indicative for overbank flow and channel fill. The pebble layers in the mudstone represent episodic flooding surfaces of pebbles, eroding the underlying sediments. Bed load transport recorded within the sandstones and conglomerate indicates high energy in the traction flow of a channel. Transport occurred mainly by traction flow along the channel floor, during which finer sediment is entrapped by graded suspension. Meters-scale medium to coarse sandstones beds that are internally cross-bedded represent lateral accretion and highlight meandering channels, while sub-horizontal conglomerate beds represent transport through a braided-style river or alluvial fan. This fifth association is therefore interpreted as a dynamic fluvial environment. The top of the Kvabebi section is mostly dominated by a conglomeratic braided river, while the top of the Kushkuna section is mainly sand-dominated and corresponds to meandering river or crevasse-splay channels.

4.1.2. Environmental changes through time

The Kvabebi and Kushkuna sections represent the most western extent of the Kura Basin and both record during the Plio-Pleistocene a general regression from nearshore to terrestrial depositional environments. The lower part of the Kushkuna section (0-60 m) records a major delta system that deposited large volumes of (volcano-)clastic material while prograding to the southeast. The upwards demise of energy in combination with soil forming processes indicated a shallowing upwards or prograding delta system.

Thereafter (60-120 m), lagoon and floodplain deposits record the appearance and increase in mollusc fauna. The most marine assemblage is found in nearshore sediments (113-120 m) that show rich marine to brackish water mollusc assemblages. The Kvabebi section similarly records nearshore sediments at its base (0-10 m), with rich and diverse brackish water faunal assemblages. Both sections are thus located near the coast of the Caspian Sea, then incurring far into the Kura Basin embayment.

The middle part of the Kvabebi section (10-165 m) and Kushkuna section (60-218 m) records vegetated floodplain or swamp deposits alternating with brackish water environments. This is interpreted as low-amplitude base-level fluctuations on a very gently sloping muddy coast. In such systems, small variations in lake-level have a large reach on coastal environments. Concentrated shell layers in the delta-top sediments represent storm transport, also evidenced by storm vortex wave ripples. Both sections display migrating channel deposits and crevasse-splay deposits, meaning active fluvial systems are nearby. The last part of the middle Kvabebi (130-165 m) and Kushkuna (205-218 m) sections marks the disappearance of brackish water molluscs fauna (Fig. 2 and 3).

The upper part of the Kvabebi section (165-280 m) and the Kushkuna section (218-300 m) is marked by increasingly more continental signatures. Sediment colour changes to yellow, brown or red signifying more oxidizing conditions. Mollusc fauna disappears completely and coarse clastic deposition becomes dominant. In Kvabebi, thick successions of braided river conglomerates are deposited. In Kushkuna, extensive soil formation and calcrete horizons are recorded, as well as numerous shallow channels. The location of the sections becomes in their upper parts further removed from the Caspian Sea and the environment becomes more dynamic and probably more erosive.

4.2. Climate reconstruction

4.2.1. Environmental impact on clay mineral assemblage

The effect of depositional environment on the clay mineral assemblage is investigated in this section by studying oriented clay mounts. The top four patterns in Figure 10a show fine-grained lithofacies Fsl and Fsm from different levels of the Kvabebi section, all reflecting the presence of quartz, illite and chlorite as most obvious constituents. The presence of kaolinite and halloysite is not immediately apparent. These patterns show

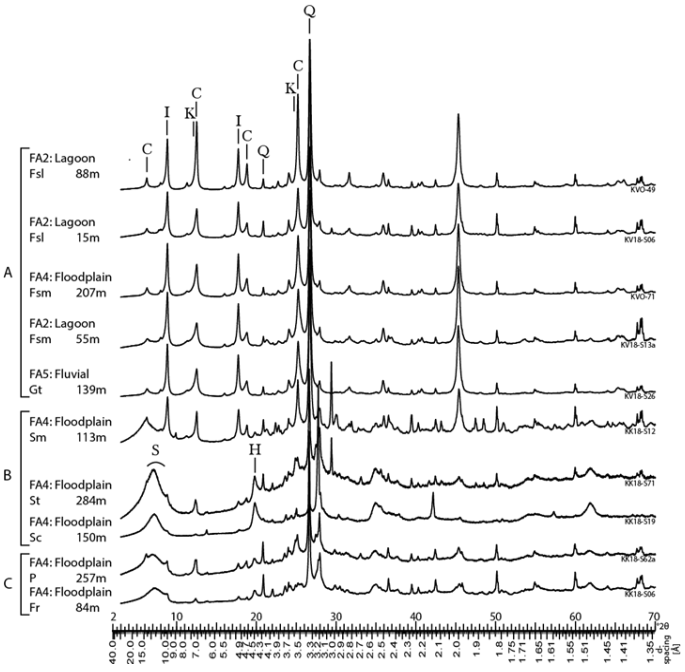

Figure 10: X-Ray diffraction pattern for oriented clay mounts showing **A)** lithofacies type is of minor influence on the pattern (all Kvabebi section); **B)** greater variety in sandy deposits from FA Floodplain (all Kushkuna section); **C)** similar patterns for fine-grained deposits of floodplain facies association, one from bottom and one from the top of the Kushkuna section. C=chlorite, I=illite, K=kaolinite, Q=quartz, H=halloysite, S=smectite or smectite mixed

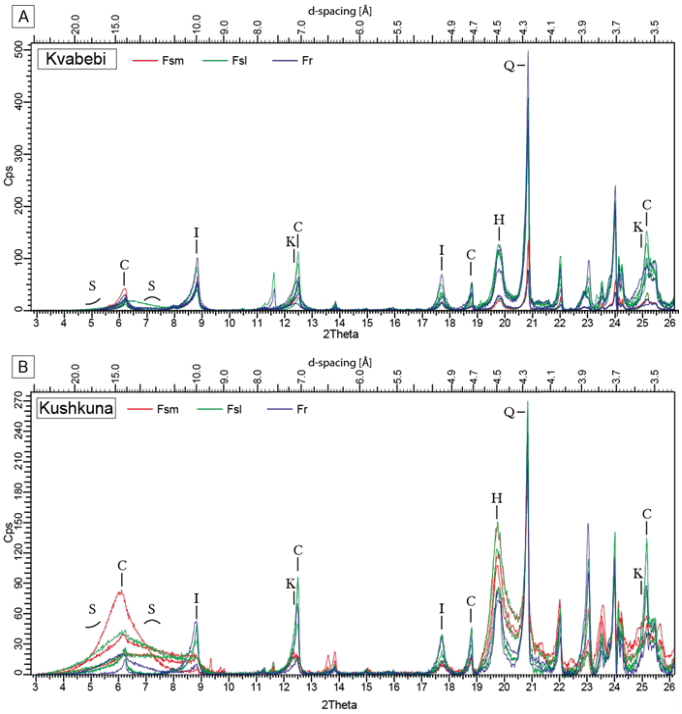

Figure 11: XRD traces of random powder measurements of fine grained lithofacies Fsm, Fsl and Fr divided per section. No relationship between peak intensities and lithofacies type is apparent, all peak intensities seem to vary independent of lithofacies type.

great similarity across the fine-grained lithofacies as well as the clay in the gravel-dominated facies Gt. The clay mineralogic composition thus seems to be largely independent of lithofacies type for mud-dominated sediments.

Sand-dominated lithofacies Sm, St, and Sc from the Kushkuna floodplain deposits show greater variety in their <10 μm fraction compared to mud-dominated deposits (Fig. 10b) but are still generally composed of quartz, illite, chlorite, kaolinite, halloysite, and smectite. The abundance of these minerals seems to vary more strongly compared to the fine-grained sediments in the Kvabebi section (Fig. 10a). This suggests that sand-dominated facies are more sensitive to lithofacies type.

The fine-grained floodplain lithofacies P and Fr, that are associated to a degree of soil-formation, show similar patterns with relatively minor differences in composition (Fig. 10c). These samples represent completely different parts of stratigraphy. This shows that within the same sedimentary environment, mineralogic composition is similar but relative abundances vary with stratigraphic position.

Random powder measurements of fine-grained lithofacies Fsm, Fsl, and Fr are compared for both sections in Figure 11. The patterns of the clay fraction show generally the same peaks, with intensity variations that do not show a preferred lithofacies but instead seem to vary independent of lithofacies type. This implies that minerals in the clay fraction in these sediments were not or little subjected to preferential deposition or neoformation. All lithofacies types consistently show high intensities for halloysite and smectite in the Kushkuna section, whilst the opposite is true for Kvabebi. Smectite is mostly absent from Kvabebi and halloysite generally minor, while illite and chlorite are consistently stronger signals compared to Kushkuna. The clearest signal for kaolinite is evident in the Kushkuna section. This discrepancy is also obvious from the mineral ratios (Fig 3b, 4b). Halloysite/chlorite and kaolinite/chlorite ratios are generally 2.5 times higher in the Kushkuna section compared to the Kvabebi section, smectite/illite even an order of magnitude. This major difference in general composition between the two sections may suggest different parent material for these sections, controlling the availability of clay minerals in these sediments.

Aside from this source rock signal, the mineralogy of the clay fraction is similar for all lithofacies studied. Sandy lithofacies Sm, St, and Sc from the Kushkuna section show greater variety, particularly in terms of abundance. The mineralogy of the clay fraction of fine-grained lithofacies can therefore be used for paleoclimate reconstructions, since the original climatic signal does not seem to have a relationship to lithofacies. Moreover, they are the most abundant lithofacies and allow for an almost continuous record along both stratigraphic records.

4.2.2. Climate evolution through time

Paleoclimate signals are derived trough semi-quantitative analysis of the most relevant clay minerals. Trends in ratios between these minerals in samples along the sections carry information on weathering patterns trough time (Fig.12). Although the data density is low, some common patterns and signals emerge from this random powder data.

In general, the trends are in phase. Especially in the Kvabebi section, the halloysite/chlorite (H/C) and kaolinite/chlorite (K/C) ratios display near-perfect similarity. In the Kushkuna section, H/C and K/C ratios are in phase up to stratigraphic level 130 m, after which they diverge. Smectite/illite (S/I) trends are mostly in phase with H/C and K/C trends but show variations at smaller scale and from 150 m in Kvabebi. H/C and K/C values are mainly increasing upwards in stratigraphy. However, values at the top of the sections return to similar values to the lower-

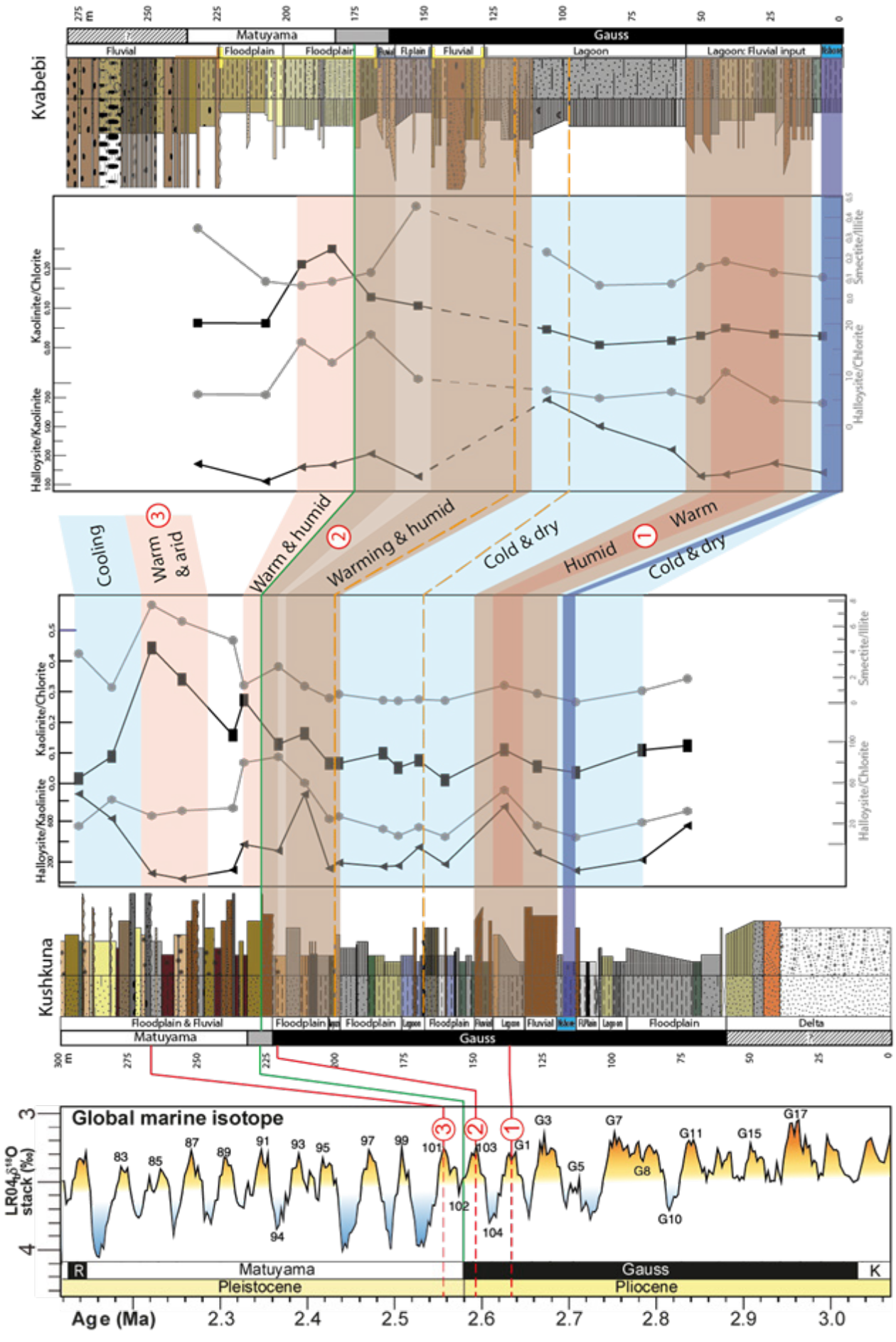

Figure 12: Proposed correlation model between the Kushkuna and Kvabebi sections based on the magnetostratigraphic time frame (green line, preliminary result of Lazerev pers.comm.), nearshore environment (dark blue shaded interval), sandy intervals (brown shading), storm beds (dashed orange line) and the clay mineralogic trends. Note that the magnitude of clay mineral ratios is not the same in both sections, owing to different sediment provenances. Light blue shaded areas indicate cold climatic conditions, red shaded areas with encircled number indicate thermal maxima. Note that the thermal maxima seem to correspond to sandy intervals. The Gauss-Matuyama polarity change and the thermal maxima are correlated to the Global Marine Isotope record (Lisiecki and Raymo 2005) and geological timescale (Gradstein, Ogg and Ogg, 2012). This correlation suggests 0.04 Ma intervals for the thermal maxima and minima, in the range of 41 Ka obliquity astronomical forcing. (for legend see Fig. 2).

most samples.

The S/I, K/C and H/C ratios represent the style of weathering in the source area. Physical weathering during colder and drier periods characteristically produces higher amounts of illite and chlorite, while chemical weathering during warmer and wetter periods produces higher amounts of smectites, kaolinite, and halloysite. The ratio halloysite/kaolinite (H/K) represents the degree of hydrolysis in the entire history of the sediment. Halloysite is a hydrated form of kaolinite and is favoured by highly hydrolysing conditions. It forms in very humid soils, where drainage is poor (Joussein et al. 2005, and references therein). When a soil is actively drained, kaolinite will replace halloysite (Meunier 2005). A high ratio of halloysite to kaolinite is thus used to indicate humid climatic conditions, while a low ratio represents drier, low water-table conditions.

The Kvabebi section records low H/C, K/C and S/I ratios from 0 to 100 m, with a maximum at 40 m. From 100 to 200 m, H/C and K/C ratios rise to their section-maximum values between 170 and 195 m, before returning to low values near the top of the sampled section (230 m). Using these ratios as temperature proxy's, the Kvabebi section records a cold interval from 0 to 100 m with a minor thermal maximum around 40 m. Climate warms from 100 to 200 m, followed by cooling until 230 m. The H/K ratio is generally low for the entire section, rising to the section-maximum from 50 to 105 m. Relatively high ratios are recorded from 170 to 195 m. Using the H/K as a humidity proxy, the Kvabebi section records generally arid conditions, with maximum humidity around 105 m and relatively humid conditions from 170 to 195 m.

The Kushkuna sections records generally low values for all ratios from 70 to 200 m, with a maximum around 190 m. H/C and K/C ratios rise to from 200 to 230 m, after which H/C ratios decrease until the end of the sampled section at 290 m. K/C and S/I ratios continue to rise until their maximum value around 270 m, before decreasing towards the end of the sampled section. Combining H/C, K/C, and S/I ratios as a temperature proxy, the Kushkuna section records cold conditions from 70 to 200 m with a thermal maximum around 190 m. Climate generally warms from 200 to 270 m with a first maximum around 230 m and an absolute maximum around 270 m. Temperatures decrease towards the end of the measured section. Adding the H/K ratio as a proxy for humidity, the Kushkuna section generally records cold and arid or warm and humid conditions, except for the interval from 210 to 280 m where this relation is inverse. While climate is warming, aridity increases and as climate cools, humidity increases.

5. Discussion

5.1. Environmental conditions in the Pliocene-Pleistocene Kura Basin

5.1.1. Geographical settings in a marginal basin of the Caspian Sea

The Kvabebi and Kushkuna sections both record mud-dominated sedimentation in near-coastal environments, alternating with sparse sandstone bodies associated with episodic fluvial input. The alternation of these environments indicates that the sea was nearby during this time. The mud-dominated deposits and the absence of tidal or major wave features indicate that tidal and wave energies were insufficient to reach the far western end of the Kura Basin embayment. Tidal and major wave energy could have been absent on the whole for the isolated Caspian Sea, as proposed by a previous research (Jorissen et al. 2019). The alternation of lagoon and floodplain deposition throughout the sections implies that the coastline was near the location of the sections for a sustained time. This is here attributed mainly to the balance between subsidence and sediment supply that kept the coastline in a relatively constant position. Whether the lake-level was constant or fluctuating and thereby controlling the position of the coastline, could not be discerned in this study. Storm events were occasionally able to transport sediment and mollusc debris far inland over the low-gradient coast. Both sedimentary records highlight a protected, shallow, muddy coastline, occasionally influenced by nearby fluvial systems. Paleocurrents in the fluvial-associated sandstones indicate a general transport direction towards the east or southeast for both sections (Fig. 9), implying that the sea must have been eastward.

These were likely separated fluvial systems, evidenced by dissimilar composition of the sediments in both sections. Clay mineralogy suggests sediments originating from different source rocks for both sections, with two distinct mineralogic signatures. The Kushkuna section displays the highest abundance of smectite and halloysite, both associated with volcanism (Meunier 2005; Chamley 1989). Halloysite is even directly associated with weathering of volcanic glass (Quantin, Gautheyrou, and Lorenzoni 1988; Kadir and Karakas 2002). The Kvabebi section displays a general higher abundance of chlorite, a mineral that tends to originate from crystalline metamorphic or igneous rocks (Chamley 1989). These diverging associations with parent rock material can be explained by different sediment provenance. Oligocene-Miocene syn-collisional mafic magmatism and Late Miocene Alkaline volcanism extend over a large area in the Lesser Caucasus (Adamia et al. 2011, and references therein). The high abundance of volcanism-related halloysite and smectite in sediments from the Kushkuna section therefore suggests a Lesser Caucasus source. The Greater Caucasus southern slope exposes Mesozoic-Early Cenozoic rocks, consisting mainly of open-marine sediments such as terrigenous fine-grained clastics, recrystallized limestones and rare volcanoclastics. These deposits have been highly deformed and underwent moderate metamorphism (Adamia et al. 2011; Saintot et al. 2006). The clay mineralogic signature of sediments in the Kvabebi section matches with a crystalline or metamorphic source rock, here identified as the Greater Caucasus. This clear separation in sediment provenance is remarkable, since the sections are presently less than 30 km apart. A topographic high related to the Kura fold-thrust belt in between the sections could have acted as a local sediment barrier, forming a divide that prevented the sediments sourced in the Greater and Lesser Caucasus to mix.

5.1.2. Environmental evolution of the marginal Kura Basin

The two studied sections were located on the westernmost margin of the Kura Basin. This marginal setting provides valuable insight regarding the extent and timing of the Caspian Sea flooding during the Akchagylian regional stage. Environmental changes are compared across the sections and to conditions in

other parts of the basin, to reconstruct the development of the Kura Basin.

The Kushkuna section records at its base a thick succession of deltaic sandstones of unknown age. Previous work (Ali-Zade et al. 1972) describes a regionally pronounced erosional unconformity that separates this package from the overlying Akchagylian deposits, suggesting that considerable geological time is missing before the onset of Akchagylian sedimentation. The sediments overlying this unconformity show first a deepening upward trend, from floodplain to its only nearshore environment (around stratigraphic level 115m), while the Kvabebi section records its only nearshore environment at its base. These nearshore environments that occur once in each section represent the most marine conditions with typical Akchagylian fauna and thus signal the maximum inland extent of the Caspian Sea recorded in these sections. Both sections record strikingly similar patterns after the nearshore environment: alternating floodplain and lagoon environments that feature two storm surfaces and two sandy intervals (Fig. 2 & 3). These features are likely all regional expressions of events: The nearshore sediments representing the maximum inland extend of the Caspian Sea, the storm surfaces representing large storms that affected both sections, and the sandy intervals representing increased sediment supply by either climate induced weathering or tectonic upheaval. If indeed regional processes that similarly affected both locations, the intervals could be correlated across the sections (Fig.12).

The alternating lagoon and floodplain environments combined with storm deposits imply that the sections were always close to the paleo-coastline. A clear transgressive surface is thus not apparent in these sections, but the full succession does seem to record the highstand deposits of the Akchagylian stage with near-coastal sedimentary environments. These sections may represent the basin-margin lateral equivalent of the Akchagylian distal mudstone-dominated environment recorded in eastern sections (Van Baak et al. 2013; Forte et al. 2014; Lazarev et al. 2019). The start of the Akchagylian transgression is dated in several sections in the eastern and interior Kura Basin to roughly 2.7 Ma (Lazarev et al. 2019; Forte et al. 2014). The Akchagylian age at the Kvabebi section of 3.3-2.7 Ma section determined by Agusti et al. (2009) seems to be conflicting with a transgression from the east to the west in the Kura Basin. To check the nature of these conflicting ages, a new paleomagnetic study was performed. New preliminary paleomagnetic data assessed along the sections in this work show that these sections record a normal polarity from the base up to stratigraphic level 170 m in Kvabebi and 225 m in Kushkuna, where polarity changes to and remains reversed for the remainder of the sections. This recorded polarity change combined with characteristic Akchagylian faunal assemblages, allows for the identification of the Gauss/Matuyama polarity switch (2.59 Ma) in these sections around stratigraphic level 170m in Kvabebi and 225m in Kushkuna. Being the only reversal recorded, no paleomagnetic age constraints can be placed on the base of the sections and thus the maximum Akchagylian age. This reversal does serve as an excellent tie-point in the correlation of the sections (Fig.12).

Both sections record an increase in coarser clastic material towards the top of the sections, and a change in environments to fluvial (paleosol formation, disappearance of aquatic molluscs) which indicates that the paleo-coastline migrates basinwards. Whether this regression is local or continues diachronously basinward to the regressive Apsheronian deposits (Lazarev et al. 2019; Forte et al. 2014; Jorissen et al. 2019) remains unresolved since stratigraphy cannot be followed above these sections. The absence of the typical Apsheronian mollusc fauna from the Kvabebi and Kushkuna sections may be either due to the absence of compatible aquatic environments in the new continental setting, or the sediments predate the appearance of the Apsheronian fauna in the Caspian Basin. The age of the topmost part of the sections is uncertain, since the Reunion magnetochron has not been sampled. Although the Reunion chron with a duration of only 20 Ky is easily missed considering the sampling resolution (5 m) in the dynamic sedimentary environments with highly variable sedimentation and erosion rates in the top part of the sections, it is more likely that these sections do not reach the Reunion. In order to determine the nature of this regressive trend, the drivers of the coarsening upward trend should be resolved. Forte et al. (2014) reported coarsening upward trends in interior basin sections that seem independent of lake-level fluctuations, but could not distinguish between increased tectonic upheaval rates in the Greater Caucasus or climatic factors causing the increased sediment input. In the following section, the climatic signal in the Kavebebi and Kushkuna sections will be explored to investigate climate as a driver of changes in sedimentary style.

5.2. Climate forcing at the Pliocene-Pleistocene boundary

5.3.1. Repeated climate changes in the Kura Basin

Clay mineralogy provides a record of climatological conditions in the catchment area of the sections. The sections share generally similar trends in climatic conditions. Clay mineralogy suggest for both sections a generally cold climate up to 200 m in Kushkuna and 115 m in Kvabebi. These cool and arid conditions are consistent with conclusions of other authors that link the Akchagylian transgression to the intensification of Northern Hemisphere Glaciations (Van Baak et al. 2019; Naidina and Richards 2018). This cold interval is interrupted by the first thermal maximum around 135 m in Kushkuna and 40 m in Kvabebi (red shaded area denoted with 1 in Fig.12). Temperatures rise across the paleomagnetic reversal in both sections to the second thermal maximum (2). These thermal maxima (1 & 2) are associated with the two sandy intervals. The increased input of coarse siliciclastic during these sandy intervals might either be the result of rejuvenation of relief due to tectonics or increased erosion rates due to wetter and warmer climate. Rejuvenation of relief causes enhanced drainage and decreased hydrolysing conditions, thus promoting the formation of kaolinite over halloysite (Meunier 2005; Joussein et al. 2005). Wet conditions and warm climate promote the formation of halloysite over kaolinite. Rejuvenation of relief as a cause of increased sediment supply should thus enforce low halloysite/kaolinite ratio's, while the opposite is observed in the sandy intervals. Therefore, we conclude that the sandy intervals result from increased erosion rates due to humidification and warming of climate.

The temperature rise across the paleomagnetic reversal in both sections coincides with major changes in sedimentary styles. In

Kvabebi, sediments change colour from grey to yellow and show higher silt, sand, and pebble contents. In Kushkuna, the succession becomes sand-dominated and colours change to brown, red, and yellow. The last and strongest thermal maximum (3) is only recorded in the Kushkuna section, owing to the impossibility to recover samples from the top 60m of the Kvabebi section. This last thermal maximum is unlike the first two, in that clay mineralogy indicates a low halloysite/kaolinite ratio. Both the low halloysite/kaolinite ratio and the increased input of coarse clastics, are now consistent with rejuvenation of relief. The climate could be simultanuously humid, but the fast upheaval of relief and increased erosion rates could have increased the drainage potential in weathering profiles, inhibiting the formation of halloysite (Meunier 2005; Joussein et al. 2005) and forcing the observed low halloysite/kaolinite ratio.

The similar climatic patters across the two sections fit the stratigraphic correlation of section 5.1.2 strikingly well, even though the sections source sediment from two different mountain ranges. This suggests that the catchment areas of the two sections were exposed to the same climatic conditions. Since the Greater Caucasus is the identified catchment area for the Kvabebi site and the Lesser Caucasus identified as the catchment area for the Kushkuna site (Section 5.1.1), the climate dominated weathering in both the Greater and Lesser Caucasus mountain ranges, suggesting a regional to global climate influence.

The climate signal in these sections is compared to the global marine isotope record in Fig.12, to investigate possible correlations based on this preliminary dataset. The climate warming across the Gauss-Matuyama paleomagnetic reversal in these sections should coincide with the transition from GIS 102 to 101 on the Pliocene-Pleistocene transition. Thermal maximum 3 can then be correlated to GIS 101 (2.56 Ma), thermal maximum 2 to GIS 103 (2.60 Ma) and thermal maximum 1 to GIS G1 (2.64 Ma). The cold intervals during the Akchagylian highstand phase might be associated with GIS 104 (2.61 Ma) and G2 (2.65 Ma). If this correlation is correct, a 0.04 My cyclicity in the range of obliquity cycles (41 ky) on temperature is recorded by clay mineralogy in the weathered sediments from both the Greater and the Lesser Caucasus, likely controlling the input of coarse clastic material to the basin margin during the Akchagylian highstand in the Kura Basin. During warm periods, sedimentation is dominated by coarser material, while cold and dry periods are dominated by mudstone deposition. Obliquity as the dominant orbital signal is consistent with Jorissen et al. (2019) who found obliquity forcing on lake-level variations in the eastern Kura Basin. The change in sedimentary style to fluvial and coarse grained towards the top of the sections is likely accompanied by increased tectonic upheaval in the Kura fold-thrust belt at the Pliocene-Pleistocene transition. Whether this regression is completely forced by increased sediment supply, or if a lowering of lake-level contributed to this trend, could not be resolved in this study. The predicted age of thermal maximum 1 (2.64 Ma) places the closest constraint on the age of the start of the Akchagylian flooding stage in this part of the Kura Basin and is consistent, if not slightly younger than the 2.7 Ma determined by other authors in more western sections (Van Baak et al. 2019, Forte et al. 2014, Lazarev et al. 2019). The nearshore environment, the most marine conditions in these sections, seems to occur in the cold interval GIS G2, dating it around 2.65 Ma. Since this interval represents the most landward position of the coastline, it might date the Maximum Flooding Surface (MFS) (Galloway 1989) of the Akchagylian highstand in the Kura Basin at 2.65 Ma.

5.3.2. Potential of continental clay mineralogy as a climate proxy

Clay mineralogy in deep-water sediments is relatively well established for the use of paleo-climatic interpretations (Biscaye 1965; Asikainen, Francus, and Brigham-Grette 2007). Complicated processes in continental deposits and availability of other methods like oxygen isotope and palynology studies caused this branch of the science to stagnate since the end of last century (Singer 1980). Nevertheless, this study argues that, with the right assumptions and detailed sedimentological framework, clay mineralogy in continental and marine marginal deposits is a valuable tool. Benefits like small sampling volume, quick analysis, and relatively low preparation costs could make this technique increasingly more popular.

Careful consideration of sedimentological conditions is indispensable for this technique. A basic comprehension of possible sediment provenance greatly enhances the interpretation of the clay mineralogic signal of the parent rock, crucial for comparison with other sites. Since the tectonic and regional settings have great impact on the clay mineral assemblage, sediment provenance, and regional structural geology are needed to provide information on the background signal. The effect of depositional environments on clay mineral assemblage is not apparent from this study. When comparing fine-grained continental or marine marginal deposits, differences in mineral composition due to environment-specific processes were imperceptible. The effect of such processes in coarse-grained clastics is likely enhanced but not further explored in this study.

The climate interpretations in this study could in the future be further compared to other data like palynology, isotope geochemistry and climate modelling to refine this technique. In general, the validity of the interpretations based solely on the clay mineralogy presented in this study may be met with ambiguity, since the sample interval is generally low due to the exploratory nature of this study. The sampling resolution in these sections can be greatly increased to provide an improved record and correlation. A general advice is to use clay mineralogy in continental settings mainly to identify low-order climatic processes, since these large-scale variations in weathering are more clearly reflected in the clay mineral composition and are less affected by differential sedimentary processes.

6. Conclusions

The Kvabebi and Kushkuna sections were examined to characterise environmental change during the Akchagylian flooding in basin margin settings, and to reconstruct climate in order to identify drivers of environmental change. The maximum westward extent of Caspian Sea in the Kura Basin was the location of the Kvabebi and Kushkuna sections, evidenced by the single occurrence of most marine “nearshore” environment. If the correlation of these sections to global climate and timescales is correct, this maximum flooding surface existed around GIS G2 (2.65 Ma). Sedimentation during the latest Pliocene was driven by climate: cold and arid intervals are dominated by mudstone

deposition, while warm and humid intervals increase the abundance of coarser grained sandstones. During the beginning of the Pleistocene, tectonic upheaval resulted in increased deposition of the coarsest-grained clastic sediment.

The paleo-coast was dominantly muddy and vegetated, evidenced by abundant plant remains. This embayment was protected from tidal and wave energy, but the sections both record two major storm events. Sediment supply balanced subsidence at least locally, so the coastline remained at roughly the same position throughout the sections, alternating between lagoon and floodplain environments. The coarsening upwards trend and the increase of sandy to conglomeratic facies towards the end of the sections is likely caused by tectonic upheaval related to the Kura fold-thrust belt, increasing the supply of weathering material to the basin margin. The marine influence terminates before the Pliocene-Pleistocene transition.

Clay mineralogy suggests a generally cold and arid climate before the Plio-Pleistocene transition. Across this transition, climate is warming and humid. The clay mineral assemblage of the Kvabebi section suggests a Greater Caucasus provenance, while the Kushkuna section sources the Lesser Caucasus. Both sections record similar climate patterns, suggesting large-scale climate trends that influenced the Greater and Lesser Caucasus similarly. Correlation to global climate suggests temperature cyclicity on obliquity timescales (41 ky).

This study shows that climate variability impacts weathering in mountainous catchment areas and thereby controls sedimentation along the coastline of this semi-enclosed basin, even during periods extreme lake-level variations. The Pliocene-Pleistocene transition in the Kura Basin margin can serve as an analogy for the present-day situation along the Caspian Sea coast, where major lake-level fluctuations are recorded in modern history during increased climate variability. The Kura Basin is also a hotspot for paleontological excavations targeting homonids. This research found most mammal remains within sandy deposits in floodplain environments. These facies are suggested to be the focus of future excavations.

This work also serves as an exploratory study in continental clay mineralogy, showing promising signs for paleo-climate reconstruction. When fine-grained deposits are concerned, the impact of the sedimentary environment seems negligible on the clay mineral assemblage. With valid assumptions and a solid sedimentary framework, climate signals can be extracted that provide additional information to data from other fields of paleo-climate research.

Acknowledgements

This research was supported by the project PRIDE (Pontocaspian RIse and DEmise), which has received funding from the European Union's Horizon 2020 research and innovation program, under the Marie Sklodowska-Curie (grant agreement Nº 642973). Maia Bukhsianidze from the Natural History Department of the Georgian National Museum and Oriol Oms from the Geological Department of the Autonomous University of Barcelona are gratefully thanked for their collaboration in the field. Technicians from the Comparative Sedimentology Laboratory (Department of Earth Sciences, Utrecht University) Coen Mulder and Anita van Leeuwen-Tolboom were of crucial importance for the success of this project. Paleomagnetic data from Sergei Lazarev and our fruitful discussions contributed to a better research work. The guidance, enthusiasm, and knowledge on clay minerals from dr. João Trabucho were invaluable and he is greatly thanked. Critical comments, constructive attitude, and great confidence from my supervisors Elisabeth Jorissen and prof. dr. Wout Krijgsman made this project a very enjoyable experience.

References

Abdullayev, Nazim R, Gregory W Riley, and Andrew P Bowman. 2012. "Regional controls on lacustrine sandstone reservoirs: the Pliocene of the South Caspian Basin." AAPG Memoires 95:71–98.

Adamia, Shota, Guram Zakariadze, Tamar Chkhotua, Nino Sadradze, Nino Tsereteli, Aleksandre Chabukiani, and Aleksandre Gventsadze. 2011. "Geology of the Caucasus: a review." Turkish Journal of Earth Sciences 20 (5): 489–544.

Agustì, J, A Vekua, O. Oms, D. Lordkipanidze, M. Bukhsianidze, G. Kiladze, and L. Rook. 2009. "The Pliocene-Pleistocene succession of Kvabebi (Georgia) and the background to the early human occupation of Southern Caucasus." Quaternary Science Reviews 28 (27-28): 3275–3280.

Ali-Zade, A.A., Alizade, K.A., Aleskerov, D.A., Buleishvili, D.A., Vekua, A.K., Konstantinova, N.A., Lebedeva, N.A., ….. (1972) "Guidebook: Excursions in Moldavia, Georgia, Azerbaijan"

Allen, JRL. 1983. "Studies in fluviatile sedimentation: bars, bar-complexes and sandstone sheets (low- sinuosity braided streams) in the Brownstones (L. Devonian), Welsh Borders." Sedimentary Geology 33 (4): 237–293.

Arpe, K, L Bengtsson, G S Golitsyn, I I Mokhov, V A Semenov, and P V Sporyshev. 2000. "Connection between Caspian Sea Level Variability and ENSO." Geophysical Research Letters 27 (17): 2693–96. https://doi.org/10.1029/1999GL002374.

Asikainen, Celeste A, Pierre Francus, and Julie Brigham-Grette. 2007. "Sedimentology, clay mineralogy and grain-size as indicators of 65 ka of climate change from El'gygytgyn Crater Lake, Northeastern Siberia." Journal of Paleolimnology 37 (1): 105–122.

Bagnold, Ralph Alger. 1946. "Motion of waves in shallow water. Interaction between waves and sand bottoms." Proceedings of the Royal Society of London. Series A. Mathematical and Physical Sciences 187 (1008): 1–18.

Bairamov, A. A., Aliyev, G. I., Hasanov, G. M., Hasanov, H. Y., Hasanov, T. A., Ismail-Zadeh, A. J., ... & Mustafayev, H. F. 2008. "Geological map of Azerbaijan Republic, 1: 500 000." National Academy of Sciences of Azerbaijan Republic-Geology Institute, Baku.

Biscaye, Pierre E. 1965. "Mineralogy and sedimentation of recent deep-sea clay in the Atlantic Ocean and adjacent seas and oceans." Geological Society of America Bulletin 76 (7): 803–832.

Bradley, W. F. (1945). "Diagnostic criteria for clay minerals." American Mineralogist: Journal of Earth and Planetary Materials, 30(11-12), 704-713.

Brunet, Marie-Fran¸coise, Maxim V Korotaev, Andrei V Ershov, and Anatoly M Nikishin. 2003. "The South Caspian Basin: a review of its evolution from subsidence modelling."

Sedimentary Geology 156 (1-4): 119–148.

Brindley, G. W., & G. Brown. 1980. "Quantitative X-ray mineral analysis of clays." Crystal structures of clay minerals and their X-ray identification, 5, 411-438.

Brown, G. 1980. "X-ray diffraction procedures for clay mineral identification." Crystal structures of clay minerals and their X-ray identification, 305-359.

Chamley, H. 1989. "Clay sedimentology." Springer Science & Business Media.

Folk, Robert L. 1966. "A review of grain-size parameters." Sedimentology 6 (2): 73–93.

Forte, A. M., Sumner, D. Y., Cowgill, E., Stoica, M., Murtuzayev, I., Kangarli, T., ... & Javakhishvili, Z. 2015. "Late Miocene to Pliocene stratigraphy of the Kura Basin, a subbasin of the South Caspian Basin: implications for the diachroneity of stage boundaries." Basin Research, 27(3), 247-271.

Gabunia, Leo, Abesalom Vekua, David Lordkipanidze, Carl C. Swisher, Reid Ferring, Antje Justus, Medea Nioradze, et al. 2000. "Earliest Pleistocene Hominid Cranial Remains from Dmanisi, Republic of Georgia: Taxonomy, Geological Setting, and Age." Science 288 (5468): 1019–25. https://doi.org/10.1126/science.288.5468.1019.

Galloway, William E. 1989. "Genetic stratigraphic sequences in basin analysis I: architecture and genesis of flooding-surface bounded depositional units." AAPG bulletin 73 (2): 125–142.

Gillet, H., Lericolais, G., & Réhault, J. P. .2007. "Messinian event in the Black Sea: Evidence of a Messinian erosional surface." Marine Geology, 244(1-4), 142-165.

Gradstein, Felix M, James George Ogg, Mark Schmitz, and Gabi Ogg. 2012. "The geologic time scale 2012." Elsevier.

Gray, Mary Beth, and Richard P Nickelsen. 1989. "Pedogenic slickensides, indicators of strain and deformation processes in redbed sequences of the Appalachian foreland." Geology 17 (1): 72–75.

Guliyev, I. S., Frantsu, Y., Muller, R., Feyzullayev, A. A., & Mamedova, S. A. 1991. "Geologic–geochemical features of oil and gas formation in the Alpine intermontane basins." Geokhimiya, 1, 148-156.

Houghton, J.T., Jenkins, G.J., and Ephraums, J.J. 1990. "Climate change: The IPCC scientific assessment". United States.

Hinds, D. J., Aliyeva, E., Allen, M. B., Davies, C. E., Kroonenberg, S. B., Simmons, M. D., & Vincent, S. J. 2004. "Sedimentation in a discharge dominated fluvial-lacustrine system: the Neogene Productive Series of the South Caspian Basin, Azerbaijan." Marine and Petroleum Geology, 21(5), 613-638.

Hoogendoorn, Robert M, Jelle F Boels, Salomon B Kroonenberg, Mike D Simmons, Elmira Aliyeva, Aliya D Babazadeh, and Dadash Huseynov. 2005. "Development of the Kura delta, Azerbaijan; a record of Holocene Caspian sea-level changes." Marine Geology 222:359–380.

Inan, S., Yalçin, M. N., Guliev, I. S., Kuliev, K., & Feizullayev, A. A. 1997. "Deep petroleum occurrences in the Lower Kura Depression, South Caspian Basin, Azerbaijan: an organic geochemical and basin modeling study." Marine and Petroleum Geology, 14(7-8), 731-762.

Jorissen, E., Abels, H., Wesselingh, F., Lazarev, S., Aghayeva, V., & Krijgsman, W. 2019. "Amplitude, frequency and drivers of Caspian Sea lake-level variations during the Early Pleistocene and their impact on a protected wave-dominated coastline". Sedimentology.

Joussein, E, S Petit, J Churchman, B Theng, D Righi, and B Delvaux. 2005. "Halloysite clay minerals–a review." Clay Minerals 40:383–426.

Kadir, Selahattin, and Zehra Karaka¸s. 2002. "Mineralogy, chemistry and origin of halloysite, kaolinite and smectite from Miocene ignimbrites, Konya, Turkey." Neues Jahrbuch fu¨r Mineralogie-Abhandlungen: Journal of Mineralogy and Geochemistry 177 (2): 113–132.

Kazmin, VG, AA Schreider, and AA Bulychev. 2000. "Early stages of evolution of the Black Sea." Geological Society, London, Special Publications 173 (1): 235–249.

Krijgsman, W., Stoica, M., Vasiliev, I., & Popov, V. V. 2010. "Rise and fall of the Paratethys Sea during the Messinian Salinity Crisis." Earth and Planetary Science Letters, 290(1-2), 183-191.

Krijgsman, W., Tesakov, A., Yanina, T., Lazarev, S., Danukalova, G., Van Baak, C. G., ... & Bruch, A. 2018. "Quaternary time scales for the Pontocaspian domain: Interbasinal connectivity and faunal evolution." Earth-science reviews 188: 1-40.

Kraus, Mary J, and Stephen T Hasiotis. 2006. "Significance of different modes of rhizolith preservation to interpreting paleoenvironmental and paleohydrologic settings: examples from Paleogene paleosols, Bighorn Basin, Wyoming, USA." Journal of Sedimentary Research 76 (4): 633–646.

Kroonenberg, Salomon B, GV Rusakov, and AA Svitoch. 1997. "The wandering of the Volga delta: a response to rapid Caspian sea-level change." Sedimentary Geology 107 (3-4): 189–209.

Kroonenberg, S. B., Alekseevski, N. I., Aliyeva, E., Allen, M. B., Aybulatov, D. N., Baba-Zadeh, A., ... & Huseynov, D. 2005. "Two deltas, two basins, one river, one sea: the modern Volga Delta an as analogue of the Neogene productive series, South Caspian Basin." SEPM Special Publication 83: 231-256.

Kroonenberg, S.B., G.M. Abdurakhmanov, E.N. Badyukova, K. van der Borg, A. Kalashnikov, N.S. Kasimov, G.I. Rychagov, A.A. Svitoch, H.B. Vonhof, and F.P. Wesselingh. 2007. "Solar-Forced 2600 BP and Little Ice Age Highstands of the Caspian Sea." Quaternary International 173–174 (October): 137–43. https://doi.org/10.1016/j.quaint.2007.03.010.

Krumbein, William C. 1936. "Application of logarithmic moments to size-frequency distributions of sediments." Journal of Sedimentary Research 6 (1): 35–47.

. 1955. "Graphic presentation and statistical analysis of sedimentary data." Recent Marine Sediments.

Lazarev, S., Jorissen, E.L., van de Velde, S., Rausch, L., Stoica, M., Wesselingh, F.P., van Baak, C.G.C., Yanina, T.A., Aliyeva, E. and Krijgsman, W. 2019. "Magnetobiostratigraphic age constraints on the palaeoenvironmental evolution of the South Caspian Basin during the Early-Middle Pleistocene (Kura Basin, Azerbaijan)".

Leroy, Suzanne A.G., Françoise Chalié, Frank P. Wesselingh, Mohammad Saeed Sanjani, Hamid A.K. Lahijani, John Athersuch, Ulrich Struck, et al. 2018. "Multi-Proxy Indicators in a Pontocaspian System: A Depth Transect of Surface Sediment in the SE Caspian Sea." Geologica Belgica 21 (3–4): 143–65. https://doi.org/10.20341/gb.2018.008.

Lisiecki, Lorraine E, and Maureen E Raymo. 2005. "A Plio-Pleistocene stack of 57 globally distributed benthic δ 18 O

records." Paleoceanography 20:1–17.

McLaren, Patrick, and Donald Bowles. 1985. "The effects of sediment transport on grain-size distribu- tions." Journal of Sedimentary Research 55 (4): 457–470.

Meunier, A. 2005. "Clays." Springer Science & Business Media.

Miall, AD. 2006. "4th Printing, The geology of fluvial deposits." Berlin, Springer-Verlag.

Mikutta, R., Kleber, M., Kaiser, K., & Jahn, R. 2005. "Organic matter removal from soils using hydrogen peroxide, sodium hypochlorite, and disodium peroxodisulfate." Soil science society of America journal, 69(1), 120-135.

Molavi-Arabshahi, M., K. Arpe, and S. A. G. Leroy. 2016. "Precipitation and Temperature of the Southwest Caspian Sea Region during the Last 55 Years: Their Trends and Teleconnections with Large-Scale Atmospheric Phenomena." International Journal of Climatology 36 (5): 2156–72. https://doi.org/10.1002/joc.4483.

Moore, D. M., & Reynolds, R. C. 1989. "X-ray Diffraction and the Identification and Analysis of Clay Minerals" Oxford university press.

Munteanu, I., Matenco, L., Dinu, C., & Cloetingh, S. 2012. "Effects of large sea-level variations in connected basins: the Dacian–Black Sea system of the Eastern Paratethys." Basin Research, 24(5), 583-597.

Nemec, W. 1988. "The Shape of the Rose." Sedimentary Geology 59 (1–2): 149–52. https://doi.org/10.1016/0037-0738(88)90105-4.

Naidina, O. D., & Richards, K. 2018. "The Akchagylian stage (late Pliocene-early Pleistocene) in the North Caspian region: Pollen evidence for vegetation and climate change in the Urals-Emba region." Quaternary International. https://doi.org/10.1016/j.quaint.2018.12.012

Nouri, J., A. R. Karbassi, and S. Mirkia. 2008. "Environmental Management of Coastal Regions in the Caspian Sea." International Journal of Environmental Science & Technology 5 (1): 43–52. https://doi.org/10.1007/BF03325996.

Nummedal, Dag, H Edward Clifton, and Eileen Williams. 2012. "Late Miocene and Early Pliocene High- Frequency Lake Level Cycles in Lacustrine Hydrocarbon Reservoir Strata, South Caspian Basin: Insights for Subseismic-scale Lithofacies Variations." 95:99–122.

O'Brien, PE, and AT Wells. 1986. "A small, alluvial crevasse splay." Journal of Sedimentary Research 56 (6): 876-879.

Ostrom, M. E. 1961. "Separation of clay minerals from carbonate rocks by using acid." Journal of Sedimentary Research, 31(1), 123-129.

Passega, Renato. 1964. "Grain size representation by CM patterns as a geologic tool." Journal of Sedimentary Research 34 (4): 830–847.

Popov, Sergej V, Irina G Shcherba, Lubov B Ilyina, Lidija A Nevesskaya, Nina P Paramonova, Sergej O Khondkarian, and Imre Magyar. 2006. "Late Miocene to Pliocene palaeogeography of the Paratethys and its relation to the Mediterranean." Palaeogeography, Palaeoclimatology, Palaeoecology 238 (1-4): 91–106.

Postma, George. 1990. "Depositional architecture and facies of river and fan deltas: a synthesis." In Coarse-grained deltas, 10:13–27.

Quantin, Paul, Jacques Gautheyrou, and P Lorenzoni. 1988. "Halloysite formation through in situ weath- ering of volcanic glass from trachytic pumices, Vico's Volcano, Italy." Clay Minerals 23 (4): 423– 437.

Reynolds, Anthony D, Michael D Simmons, Michael BJ Bowman, Jonathan Henton, Andrew C Brayshaw, Akif A Ali-Zade, Ibrahim S Guliyev, Safura F Suleymanova, Elmira Z Ateava, Dilara N Mamedova, et al. 1998. "Implications of outcrop geology for reservoirs in the Neogene Productive Series: Apsheron Peninsula, Azerbaijan." AAPG bulletin 82 (1): 25–49.

Saintot, Aline, Marie-Fran¸coise Brunet, Fedor Yakovlev, Michel S´ebrier, Randell Stephenson, Andrei Ershov, Fran¸coise Chalot-Prat, and Tommy McCann. 2006. "The Mesozoic-Cenozoic tectonic evolution of the Greater Caucasus." Geological Society, London, Memoirs 32 (1): 277–289.

Singer, Arieh. 1980. "The paleoclimatic interpretation of clay minerals in soils and weathering profiles." Earth-Science Reviews 15 (4): 303–326.

Sohn, YK. 1997. "On traction-carpet sedimentation." Journal of Sedimentary Research 67 (3): 502–509.

Sosdian, S., and Y. Rosenthal. 2009. "Deep-Sea Temperature and Ice Volume Changes Across the Pliocene-Pleistocene Climate Transitions." Science 325 (5938): 306–10. https://doi.org/10.1126/science.1169938.

Sosson, M., Rolland, Y., Müller, C., Danelian, T., Melkonyan, R., Kekelia, S., ... & Galoyan, G. 2010. "Subductions, obduction and collision in the Lesser Caucasus (Armenia, Azerbaijan, Georgia), new insights." Geological Society, London, Special Publications, 340(1), 329-352.

Sun, Donghuai, J Bloemendal, DK Rea, J Vandenberghe, Fuchu Jiang, Zhisheng An, and Ruixia Su. 2002. "Grain-size distribution function of polymodal sediments in hydraulic and aeolian environments, and numerical partitioning of the sedimentary components." Sedimentary geology 152 (3-4): 263–277.

Svedberg, T., & Nichols, J. B. 1923. "Determination of size and distribution of size of particle by centrifugal methods." Journal of the American Chemical Society, 45(12), 2910-2917.

Todd, Simon P. 1989. "Stream-driven, high-density gravelly traction carpets: possible deposits in the Trabeg Conglomerate Formation, SW Ireland and some theoretical considerations of their origin." Sedimentology 36 (4): 513–530.

Van Baak, C. G., Vasiliev, I., Stoica, M., Kuiper, K. F., Forte, A. M., Aliyeva, E., & Krijgsman, W. 2013. "A magnetostratigraphic time frame for Plio-Pleistocene transgressions in the South Caspian Basin, Azerbaijan." Global and Planetary Change, 103, 119-134.

Van Baak, Christiaan GC, Arjen Grothe, Keith Richards, Marius Stoica, Elmira Aliyeva, Gareth R Davies, Klaudia F Kuiper, and Wout Krijgsman. 2019. "Flooding of the Caspian Sea at the inten- sification of Northern Hemisphere Glaciations." Global and Planetary Change 174:153–163.

Van Wagoner, J. C., Mitchum, R. M., Campion, K. M., & Rahmanian, V. D. 1990. "Siliciclastic sequence stratigraphy in well logs, cores, and outcrops: concepts for high-resolution correlation of time and facies." AAPG Methods in Exploration Series 7

Vekua, Abesalom, David Lordkipanidze, G. Philip Rightmire, Jordi Agusti, Reid Ferring, Givi Maisuradze, Alexander

Mouskhelishvili, et al. 2002. "A New Skull of Early Homo from Dmanisi, Georgia." Science 297 (5578): 85–89. https://doi.org/10.1126/science.1072953.

Vincent, Stephen J, Clare E Davies, Keith Richards, and Elmira Aliyeva. 2010. "Contrasting Pliocene fluvial depositional systems within the rapidly subsiding South Caspian Basin; a case study of the palaeo-Volga and palaeo-Kura river systems in the Surakhany Suite, Upper Productive Series, onshore Azerbaijan." Marine and Petroleum Geology 27 (10): 2079–2106.

Vincent, Stephen J, Andrew C Morton, Andrew Carter, Samantha Gibbs, and Teimuraz G Barabadze. 2007. "Oligocene uplift of the Western Greater Caucasus: an effect of initial Arabia–Eurasia colli- sion." Terra Nova 19 (2): 160–166.

Visher, Glenn S. 1969. "Grain size distributions and depositional processes." Journal of Sedimentary Research 39 (3).

Yanina, T. A. 2014. "The Ponto-Caspian region: environmental consequences of climate change during the Late Pleistocene." Quaternary International, 345, 88-99.

Yanina, T. A.; Svitoch, A. A.; Wesselingh, F. P. 2010. "Biodiversity of the Caspian Sea mollusks during the last 10 ky." Proceedings of the International Conference "The Caspian Region: Environmental Consequences of the Climate Change. p. 138-142.